arXiv:1610.01100v1 [cond-mat.mes-hall] 4 Oct 2016

Coulomb drag between helical Luttinger liquids

N. Kainaris,[1,2] I. V. Gornyi,[1,2,3,4] A. Levchenko,[5] and D. G. Polyakov[1]

[1] *Institut für Nanotechnologie, Karlsruhe Institute of Technology, 76021 Karlsruhe, Germany*
[2] *Institut für Theorie der Kondensierten Materie, Karlsruher Institut für Technologie, 76128 Karlsruhe, Germany*
[3] *A.F. Ioffe Physico-Technical Institute, 194021 St. Petersburg, Russia*
[4] *L.D. Landau Institute for Theoretical Physics, 119334 Moscow, Russia*
[5] *Department of Physics, University of Wisconsin-Madison, Madison, Wisconsin 53706, USA*

We theoretically study Coulomb drag between two helical edges with broken spin-rotational symmetry, such as would occur in two capacitively coupled quantum spin Hall insulators. For the helical edges, Coulomb drag is particularly interesting because it specifically probes the inelastic interactions that break the conductance quantization for a single edge. Using the kinetic equation formalism, supplemented by bosonization, we find that the drag resistivity ρ_D exhibits a nonmonotonic dependence on the temperature T. In the limit of low T, ρ_D vanishes with decreasing T as a power law if intraedge interactions are not too strong. This is in stark contrast to Coulomb drag in conventional quantum wires, where ρ_D diverges at $T \to 0$ irrespective of the strength of repulsive interactions. Another unusual property of Coulomb drag between the helical edges concerns higher T for which, unlike in the Luttinger liquid model, drag is mediated by plasmons. The special type of plasmon-mediated drag can be viewed as a distinguishing feature of the helical liquid—because it requires peculiar Umklapp scattering only available in the presence of a Dirac point in the electron spectrum.

I. INTRODUCTION

The helical Luttinger liquid (HLL) emerges at the edge of a two-dimensional quantum spin Hall (QSH) insulator [1–6] and consists, in its most conventional form protected by time-reversal symmetry, of two counterpropagating Kramers conjugate modes. In an "ideal" helical edge, the electron spin is conserved for each of the chiral modes ("S_z-conserving models"). Electron-electron backscattering between the modes, as well as backscattering by nonmagnetic inhomogeneities, is then prohibited by the combination of the spin-axial and time-reversal symmetries. As a consequence, charge transport through the ideal helical edge is characterized by a quantized conductance $G_0 = 2e^2/h$, independent of the temperature T, also in the presence of nonmagnetic disorder. Experimentally, the conductance quantization has been observed at the edges of HgTe/CdTe [7, 8] and InAs/GaSb [9–11] quantum wells.

In a more realistic description of topological insulator materials, spin-rotational invariance is not preserved in the helical edge. One perturbation that violates the invariance is Rashba-type spin-orbit coupling induced by broken inversion symmetry about the plane of the semiconductor heterostructure. In the presence of nonmagnetic disorder, *elastic* backscattering between Kramers partners remains exactly forbidden by time-reversal symmetry, irrespective of the presence or absence of spin-rotational invariance. As a result, the $T = 0$ conductance is given by G_0 independently of the strength of disorder (as long as the two-dimensional bulk is insulating). However, at nonzero T, *inelastic* backscattering is generically triggered beyond the S_z-conserving models [12] and gives rise to dissipation, even in the absence of disorder, modifying significantly the transport properties of both a clean and disordered helical liquid [13]. In the limit of low T, inelastic backscattering leads to T dependent corrections to the quantized edge conductance [12, 14]. These behave, generically, as power laws of T, similar to the conventional Tomonaga-Luttinger liquid (TLL). In the thermodynamic limit, the corrections to the conductance convert into a finite conductivity [15–17] that is a power-law function of T [18]. Strong repulsive interactions are expected to block zero-T transport through the edge by spontaneously breaking time-reversal symmetry and gapping the edge modes [19]. Experimental evidence pointing towards the importance of the TLL effects in transport through a strongly interacting HLL has recently been reported [20].

In this paper, we investigate Coulomb drag between parallel clean (no disorder) edges of two identical QSH insulators, brought in proximity to each other, in the case of broken spin-rotational invariance. We assume that each of the edges consists of a single pair of Kramers partners with a linear dispersion relation. In a Coulomb drag measurement, current is driven in an "active" conductor (active edge in our setup), inducing an electrical field or current in a "passive" conductor (passive edge), with the frictional force being due to electron-electron interactions, without transfer of electrons between the subsystems. As such, Coulomb drag is a sensitive probe of inelastic electron-electron scattering. For helical edges, Coulomb drag is particularly worthy of study because, as already mentioned above, inelastic electron-electron scattering is the only source of dissipation inside a single edge.

The key quantity characterizing friction is the drag resistivity,

$$\rho_D = -E_2/j_1 \ , \tag{1}$$

where j_1 is the current density driven in the active conductor and E_2 is the electric field applied to the

passive conductor to compensate for the friction force and maintain zero current therein. In conventional one-dimensional (1D) systems (single-channel quantum wires), Coulomb drag has been intensively studied both theoretically [21–35] and experimentally [36–42]. In general, Coulomb drag in one dimension, independently of the particular form of the electron dispersion relation, can only occur in the presence of scattering that changes the chirality of electrons [34]. Therefore, there is no Coulomb drag between clean ideal HLLs, in which scattering between left- and right movers is strictly prohibited. Conversely, Coulomb drag between HLLs is only possible if there is a perturbation that breaks spin-rotational invariance of the edge modes.

One possibility to break the axial spin symmetry and lift the restriction on backscattering interactions between two helical liquids is to apply an external magnetic (Zeeman) field (the magnetic field also breaks time reversal symmetry and generically gaps the edge modes). Coulomb drag between helical liquids in the presence of a magnetic field h perpendicular to the spin-locking axis was studied in Ref. [43]. Above the temperature at which a zigzag-ordered charge density wave is formed (and for sufficiently small h, so that the electron spectrum can be approximated as linear), Ref. [43] found $\rho_D \propto h^4 T^{4K_- -3}$, where K_- is the Luttinger constant for the relative charge mode. The power-law exponent of the T dependence is here the same as for Coulomb drag between spinless TLLs, but ρ_D is strongly suppressed, compared to the TLL case, in the limit of small h.

Another possibility to destroy the spin-rotational invariance originates from spin-orbit coupling in the bulk of the spin Hall insulator. This is the model that we study in this paper, within the framework introduced in Ref. [12] for a single helical edge. Of central importance to us is that, in contrast to the magnetic field-induced drag [43], time-reversal symmetry is preserved in this model, so that the topological nature of the edge states as Kramers partners remains intact. The significance of this distinction is that Coulomb drag between helical liquids, if it is facilitated by spin-orbit coupling, differs in an essential way both from Coulomb drag induced by the Zeeman field and from Coulomb drag between TLLs.

Regarding this distinction, two most important points to emphasize are the following. First, the strong suppression of electron-electron backscattering in the limit of low T makes the formation of a strong-coupling ground state, which is a hallmark of the TLL with repulsive interactions (where a zigzag-ordered charge density wave is inevitably formed in the low-T limit), only possible if the strength of interactions exceeds a critical value. Below the critical value, ρ_D vanishes with decreasing T, in contrast to the TLL case. Second, time-reversal symmetry necessitates the existence of a Dirac point in the HLL spectrum. In the vicinity of the Dirac point, Umklapp scattering contributes to Coulomb drag in addition to backscattering. This results in the emergence of a peculiar regime of plasmon-mediated Coulomb drag at higher T.

To make a systematic treatment of the peculiarities of Coulomb drag between helical liquids, we formalize our approach from two complementary perspectives. We first study the kinetic equation for weakly interacting helical fermions. Having established—for the case of weak interactions—the vanishing of ρ_D in the limit of low T and the dominance of plasmon-mediated drag for higher T, we proceed to bosonize the model and include the TLL renormalization effects using the Kubo formula.

The paper is organized as follows. In Sec. II, we formulate the model of two capacitively coupled helical edges with broken spin-rotational symmetry. Section III is devoted to the study of Coulomb drag between weakly-interacting edges within the kinetic equation approach. We write down the kinetic equation for two-particle scattering in the helical edges in Sec. III A. The high- and low-frequency regimes of Coulomb drag are considered in Secs. III B and III F, respectively. In Sec. III C, we discuss dynamically screened interaction in the helical edges. In Secs. III D and III E, we obtain, respectively, the electron-hole and plasmon contributions to the drag rate. In Sec. IV, we address the effects of strong intraedge interaction on the drag resistivity within the bosonization framework. The renormalization of the first- and second-order backscattering amplitudes is analyzed in Secs. IV A and IV B, respectively. Section IV C deals with the renormalization of the drag resistivity. The strong coupling regime is discussed in Sec. IV D. Section V concludes with a summary. Some of the technical details are moved to the Appendices.

Throughout, we use the abbreviation $\int_k = \int \frac{\mathrm{d}k}{2\pi}$.

II. THE MODEL

We start by formulating our model for two helical liquids with broken spin-rotational invariance coupled by a screened Coulomb interaction. In substance, we employ the model proposed—for a single helical edge—in Ref. [12] and extend it to the case of two edges. We consider two identical QSH systems at the same chemical potential μ, each with one Kramers pair at the edge, as shown in Fig. 1. Tunneling between the two QSH systems is neglected. The transverse size of the edge channels is assumed to be much smaller than the interedge distance d. We focus on Coulomb drag between infinitely long edges, i.e., the wavevector of the external perturbation in the response functions is sent to zero before taking the dc limit: this is the order of limits that defines the dc resistivity in general, and the dc drag resistivity ρ_D in particular.

The kinetic part H_0 of the Hamiltonian is given by

$$H_0 = \sum_{\sigma\eta} \int_k (v\eta k - \mu)\, \psi^\dagger_{k\sigma\eta} \psi_{k\sigma\eta} \ , \tag{2}$$

where $\psi_{k\sigma\eta}$ is the electron operator at the momentum k in edge $\sigma = 1, 2$ with the chirality $\eta = \pm$, and v is

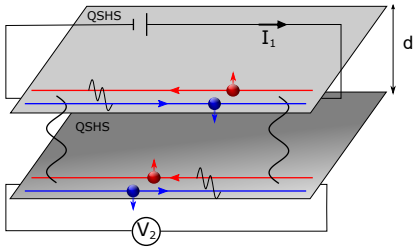

FIG. 1. Schematics of a Coulomb drag measurement between helical edges of two QSH systems. Current I_1 is driven through the active edge and, as a result of electron-electron interactions, voltage V_2 is induced in the passive edge.

the velocity in the linear dispersion relation. The sum over k for each of the chiralities runs from $-\infty$ to ∞ (the bandwidth of the edge states is assumed to be larger than all other relevant energy scales), with the chiral spectral branches crossing at $k = 0$ ("Dirac point").

In the ideal helical edge, the spin-locking axis is independent of k, so that the electron state $\tilde{\psi}_{k\sigma s}$ with a given spin projection $s =\uparrow,\downarrow$ coincides with $\psi_{k\sigma\eta}$. As already discussed in Sec. I, we specialize to the model in which the spin-rotational invariance of the helical edges is broken by Rashba-type spin-orbit coupling in the bulk. In the absence of spin-axial symmetry, $\tilde{\psi}_{k\sigma s}$ is generically a mixture of the chiral states $\psi_{k\sigma\eta}$ with both chiralities η. By time-reversal symmetry, the unitary transformation between the two basis sets ("spin" vs "chiral") in the vicinity of the Dirac point has a universal form, as far as the dependence on k is concerned, to order $\mathcal{O}(k^2)$. Specifically [12],

$$\begin{aligned}\tilde{\psi}_{k\sigma\uparrow} &\simeq \psi_{k\sigma+} - \frac{k^2}{k_0^2}\psi_{k\sigma-} \ , \\ \tilde{\psi}_{k\sigma\downarrow} &\simeq \psi_{k\sigma-} + \frac{k^2}{k_0^2}\psi_{k\sigma+} \ ,\end{aligned} \tag{3}$$

where k_0 is a model-dependent momentum scale which characterizes the strength of spin-orbit coupling (taken to be identical in the two edges). We assume that the spin-orbit interaction is a weak symmetry-breaking perturbation with $vk_0 \gg \max\{|\mu|, T\}$, so that the quadratic-in-k expansion (3) is sufficient for our purposes (here and below, we count μ from the Dirac point).

The density-density interaction term in the Hamiltonian is then written in the chiral basis, rotated with respect to the spin basis according to Eq. (3), as

$$\begin{aligned}H_{\rm int} = \frac{1}{2}\sum_{\sigma\sigma'\eta_1\eta_2\eta_3\eta_4}\int_{kk'q} b_{\eta_1\eta_4}(k+q,k)b_{\eta_2\eta_3}(k'-q,k') \\ \times V_{\sigma\sigma'}(q)\,\psi^\dagger_{k+q,\sigma\eta_1}\psi^\dagger_{k'-q,\sigma'\eta_2}\psi_{k'\sigma'\eta_3}\psi_{k\sigma\eta_4} \ ,\end{aligned} \tag{4}$$

where $V_{\sigma\sigma'}(q)$ is the Fourier component of the interaction potential inside ($\sigma = \sigma'$ equal to 1 or 2) and between ($\sigma \neq \sigma'$) the edges and

$$b_{\eta_1\eta_2}(k_1,k_2) = \delta_{\eta_1\eta_2} - \eta_1\delta_{\eta_1,-\eta_2}\frac{k_1^2-k_2^2}{k_0^2} \ . \tag{5}$$

We assume that the interactions in the double-edge system are screened by a nearby metallic gate. Note that—irrespective of the relation between the distance to the gate and the distance between the wires d—the inter-wire potential $V_{12}(q)$ starts to decay exponentially with increasing $|q|$ at $|q| \sim 1/d$ (see, e.g., Appendix A of Ref. [34]). For simplicity, we take $V_{11}(q) = V_{22}(q)$ to be given by a constant $V_{0\parallel}$ and $V_{12}(q)$ by a simple exponential $V_{0\perp}e^{-|q|d}$. Throughout Sec. III, we also assume that $V_{0\parallel} = V_{0\perp}$.

The presence of the factors (5) in the interacting part of the Hamiltonian for the helical liquid constitutes the key difference between the helical and conventional Luttinger models. Another difference to notice is related to the population of the eigenstates at thermal equilibrium. The conventional Luttinger model is formulated for $T \ll |\mu|$, where the chemical potential μ is counted from the energy at which the chiral spectral branches meet [either at the bottom of the electron spectrum, linearized in the vicinity of the Fermi energy, or at the crossing point of two chiral branches with a linear dispersion relation, similarly to Eq. (2)]. In the helical Luttinger model, we assume that T can be larger than the energy difference between the Fermi level and the Dirac point, so that the real scattering processes that involve the electron states at and around the Dirac point are not necessarily thermally suppressed.

III. COULOMB DRAG BETWEEN HELICAL EDGES: KINETIC THEORY

As mentioned in Sec. I, we first consider Coulomb drag between helical edges within the kinetic equation framework in the limit of weak interactions, by neglecting the TLL renormalization of the parameters of the system. This is the same limit that was studied in Ref. [12] for a single edge. As will be seen below, the double-edge system for the case of weak interactions exhibits an essentially richer behavior—as far as the transport mechanisms are concerned—than the single edge, primarily because of an important subtlety in the plasmon-mediated coupling between the edges.

A. Kinetic equation

The kinetic equation for f_σ, the distribution function in edge σ, reads

$$\partial_t f_\sigma(1) - eE_\sigma\partial_{k_1} f_\sigma(1) = {\rm St}_\sigma(1) \ , \tag{6}$$

where E_σ is the electric field ($e > 0$) in edge σ and the argument of $f_\sigma(1)$ includes both the momentum and chirality, with 1 being a shorthand notation for k_1 and η_1,

etc. As a starting point, we neglect intraedge collisions (these will be included in Sec. III F) and write the collision integral $\mathrm{St}_\sigma(1)$ for pair collisions as (for $\sigma = 1$)

$$\mathrm{St}_1(1) = (2\pi)^2 \sum_{\eta_2\eta_{1'}\eta_{2'}} \int_{k_2 k_{1'} k_{2'}} \left|V_{12}(k_{1'}-k_1, \epsilon_{1'}-\epsilon_1)\right|^2 |b_{\eta_{1'}\eta_1}(k_{1'},k_1)|^2 |b_{\eta_{2'}\eta_2}(k_{2'},k_2)|^2\, \delta(k_1+k_2-k_{1'}-k_{2'}) \\ \times \delta(\epsilon_1+\epsilon_2-\epsilon_{1'}-\epsilon_{2'}) \left\{ f_1(1')f_2(2')[1-f_1(1)][1-f_2(2)] - f_1(1)f_2(2)[1-f_1(1')][1-f_2(2')] \right\} \tag{7}$$

where $\epsilon_1 = v\eta_1 k_1$, etc. The collision integral $\mathrm{St}_2(1)$ for electrons in edge 2 is obtained by exchanging the edge indices $1 \leftrightarrow 2$ of the distribution functions. The dynamically screened RPA interaction $V_{12}(q,\Omega)$, whose derivation is given in Appendix A, is specified in Eq. (23) below. As will be shown in Sec. III E, screening plays a crucial role in the present problem for not too low T as it opens up a peculiar plasmon-mediated scattering channel for Coulomb drag.

It is convenient to represent $f_\sigma(1)$ in terms of the function $g_\sigma(1)$ as

$$f_\sigma(1) = n_F(\epsilon_1) - g_\sigma(1) n_F(\epsilon_1)[1-n_F(\epsilon_1)]\,, \tag{8}$$

where $n_F(\epsilon_1) = [1+\exp(\epsilon_1-\mu)/T]^{-1}$ is the thermal distribution function. Linearizing Eq. (6) in g_σ, we obtain (in the ω representation)

$$-i\omega g_\sigma(1) - \eta_1 \frac{eE_\sigma v}{T} = \mathrm{st}_\sigma(1)\ , \tag{9}$$

where (for $\sigma = 1$)

$$\mathrm{st}_1(1) = \frac{4}{\zeta^2(1)} (2\pi)^2 \sum_{\eta_2\eta_{1'}\eta_{2'}} \int_{k_2 k_{1'} k_{2'}} \left|V_{12}(k_{1'}-k_1, \epsilon_{1'}-\epsilon_1)\right|^2 \left|b_{\eta_{2'}\eta_2}(k_{2'},k_2)\right|^2 \left|b_{\eta_{1'}\eta_1}(k_{1'},k_1)\right|^2 \delta(\epsilon_1+\epsilon_2-\epsilon_{1'}-\epsilon_{2'}) \\ \times \delta(k_1+k_2-k_{1'}-k_{2'})\, n_F(\epsilon_1) n_F(\epsilon_2)[1-n_F(\epsilon_{1'})][1-n_F(\epsilon_{2'})]\,[\,g_1(1')+g_2(2')-g_1(1)-g_2(2)\,]\ . \tag{10}$$

and

$$\zeta(1) = \frac{1}{\cosh[(\epsilon_1-\mu)/2T]}\ . \tag{11}$$

The electric current in edge σ, as a linear response to the fields E_σ, is related to the solution of Eq. (9) by

$$j_\sigma = \frac{ev}{4} \sum_{\eta_1} \eta_1 \int_{k_1} \zeta^2(1)\, g_\sigma(1)\ . \tag{12}$$

The dc drag resistivity ρ_D is conventionally defined in terms of j_σ and E_σ as in Eq. (1). For the discussion in Sec. III B, we introduce also the ω-dependent drag conductivity defined as

$$\sigma_{12} = j_1/E_2 \tag{13}$$

under the condition that $E_1 = 0$.

B. High-frequency Coulomb drag: Scattering rate

In the limit of large ω, Eq. (9) can be solved for $g_\sigma(k,\eta)$ iteratively by expanding the solution in powers of $1/\omega$. Neglecting collisions between particles ($\mathrm{st}_\sigma \to 0$) gives

$$g_\sigma^{(0)}(k,\eta) = \frac{1}{-i\omega+0}\, \eta\, \frac{eE_\sigma v}{T}\ . \tag{14}$$

By substituting Eq. (14) in st_σ, the dissipative part of σ_{12} [Eq. (13)] for large ω is then obtained, to order $1/\omega^2$, as

$$\mathrm{Re}\,\sigma_{12} \simeq -\frac{e^2 v}{\pi\omega^2 \tau_D^\infty}, \qquad \omega\tau_D^\infty \gg 1\ , \tag{15}$$

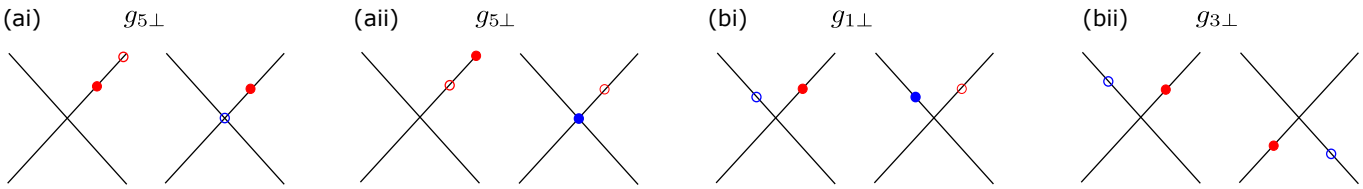

FIG. 2. Momentum configurations for two-particle scattering in channels (a) and (b) [defined in Eq. (17)] and the corresponding g-ology classification. Occupied and unoccupied states are depicted as filled and empty circles, respectively. Blue (red) circles denote left (right) movers. For $g_{5\perp}$ processes (channel a), the left mover is at zero energy while the right movers are close to the Fermi surface. As explained in the text, the contributions to the drag rate of processes (ai) and (aii) cancel each other. The drag rate is determined by $g_{1\perp}$ and $g_{3\perp}$ processes.

where

$$\frac{1}{\tau_D^\infty} = -\frac{(2\pi)^3}{T}\sum_{\eta_1\eta_2\eta_{1'}}\int_{k_1k_2k_{1'}k_{2'}}\eta_1\eta_2\left|V_{12}(k_{1'}-k_1,\epsilon_{1'}-\epsilon_1)\right|^2\left|b_{-\eta_2,\eta_2}(k_{2'},k_2)\right|^2\left|b_{\eta_{1'}\eta_1}(k_{1'},k_1)\right|^2 \\ \times\,\delta[\,\eta_1k_1+\eta_2(k_2+k_{2'})-\eta_{1'}k_{1'}]\,\delta(k_1+k_2-k_{1'}-k_{2'})\,n_F(\epsilon_1)n_F(\epsilon_2)[1-n_F(\epsilon_{1'})][1-n_F(-v\eta_2k_{2'})]\,. \tag{16}$$

The symbol ∞ here is used to emphasize that the "drag rate" $1/\tau_D^\infty$ is calculated in the high-frequency limit. Importantly, since $g_\sigma^{(0)}$ is independent of k, backscattering of at least one particle involved in the collision process is required to produce a nonzero drag rate. Specifically, the $1/\tau_D^\infty$ is a sum of contributions of four scattering channels:

$$\begin{array}{ll} \text{(ai)}\ \ \eta_1=\eta_{1'}\ \text{ and }\ \eta_2=\eta_1\ , & \text{(bi)}\ \ \eta_1=-\eta_{1'}\ \text{ and }\ \eta_2=-\eta_1\ , \\ \text{(aii)}\ \ \eta_1=\eta_{1'}\ \text{ and }\ \eta_2=-\eta_1\ , & \text{(bii)}\ \ \eta_1=-\eta_{1'}\ \text{ and }\ \eta_2=\eta_1\ . \end{array} \tag{17}$$

The different scattering channels are depicted in Fig. 2 (together with their g-ology classification).

The scattering processes (ai) and (aii) correspond to $g_{5\perp}$ scattering in the g-ology classification, with one of the scattering states being tied to the Dirac point. Denoting $k_1-k_{1'}=q$, we have for the two contributions to $1/\tau_D^\infty$:

$$R_{\rm ai} = -\frac{\pi}{T}\sum_{\eta_1}\int_{k_1q}\left|V_{12}(q,vq)\right|^2\left(\frac{q}{k_0}\right)^4 n_F(\epsilon_1)n_F(v\eta_1q)\,\{1-n_F[v\eta_1(k_1+q)]\}\,[1-n_F(0)] \tag{18}$$

$$R_{\rm aii} = \frac{\pi}{T}\sum_{\eta_1}\int_{k_1k_{1'}}\left|V_{12}(q,vq)\right|^2\left(\frac{q}{k_0}\right)^4 n_F(\epsilon_1)n_F(0)\,\{1-n_F[v\eta_1(k_1+q)]\}\,[1-n_F(-v\eta_1q)]\ . \tag{19}$$

These are seen to cancel out, $R_{\rm ai}=-R_{\rm aii}$. This is because the initial states for one of the two channels of $g_{5\perp}$ scattering are the final states for the other (Fig. 2), so that the product of the thermal factors is the same for both channels, namely

$$n_F(\epsilon_1)n_F(v\eta_1q)\,\{1-n_F[v\eta_1(k_1+q)]\}\,[1-n_F(0)] = n_F(\epsilon_1)n_F(0)\,\{1-n_F[v\eta_1(k_1+q)]\}\,[1-n_F(-v\eta_1q)]\ , \tag{20}$$

whereas the transferred momenta are of opposite sign.

The high-frequency drag rate is thus determined by the remaining sum of the contributions of the (bi) and (bii) processes, which correspond to $g_{1\perp}$ backscattering and $g_{3\perp}$ Umklapp scattering, respectively:

$$\frac{1}{\tau_D^\infty} = \frac{4\pi}{Tk_0^8}\int_{qQ}Q^4q^4\left|V_{12}(q,2vQ)\right|^2W(q,Q)\ , \tag{21}$$

where

$$W(q,Q) = \frac{1}{\cosh\frac{vq-2\mu}{2T}+\cosh\frac{vQ}{T}}\left[\frac{1}{\cosh\frac{vq-2\mu}{2T}+\cosh\frac{vQ}{T}}-\frac{1}{\cosh\frac{vq+2\mu}{2T}+\cosh\frac{vQ}{T}}\right]+(q\to-q) \tag{22}$$

and $2Q=k_1+k_{1'}$ is the total momentum of the incoming (k_1) and outgoing ($k_{1'}$) particles in edge 1. The energy-momentum conservation fixes the transferred frequency

in the RPA interaction at $\epsilon_1 - \epsilon_{1'} = 2vQ$.

The $g_{1\perp}$ and $g_{3\perp}$ contributions to $1/\tau_D^\infty$ [which are given by the first and second terms in the square brackets in Eq. (21), respectively] are of opposite sign, but—in contrast to the $g_{5\perp}$ processes, whose contribution to the drag rate vanishes exactly for arbitrary μ—they generically do not cancel each other exactly. Note that they do so, however, at the particle-hole symmetric point $\mu = 0$.

C. Dynamically screened interaction

Before proceeding with the calculation of the drag rate, let us elaborate on the importance of the dynamical part of the screened RPA interaction $V_{12}(q, 2v_F Q)$ in Eq. (21). Derived in Appendix A, $V_{12}(q,\Omega)$ reads

$$V_{12}(q,\Omega) = \frac{V_0 e^{-|q|d}\left[(vq)^2 - \Omega^2\right]^2}{\left[(\Omega + i\Gamma_+)^2 - \Omega_+^2\right]\left[(\Omega + i\Gamma_-)^2 - \Omega_-^2\right]} , \tag{23}$$

where the dispersion relation for the symmetric (+) and antisymmetric (−), in the edge index, plasmon modes is given by

$$\Omega_\pm(q) = v_\pm(q)|q| \tag{24}$$

with the velocities

$$v_\pm(q) = \sqrt{1 + \alpha_\pm(q)}\, v \tag{25}$$

[see also Eq. (77) for the excitation spectrum of the bosonized Hamiltonian] and

$$\alpha_\pm(q) = \alpha\left(1 \pm e^{-|q|d}\right) , \tag{26}$$

with $\alpha = V_0/\pi v$ being the dimensionless strength of intrawire interactions. It is assumed here that the Fourier components of the intraedge and interedge bare potentials at zero momentum [$V_{0\parallel}$ and $V_{0\perp}$ below Eq. (5), respectively] are the same, so that the velocity of the antisymmetric plasmon at $q = 0$ is not renormalized by interactions; this makes the calculation less cumbersome without changing the result qualitatively. The plasmon damping rate $\Gamma_\pm(q)$ is induced by chirality-changing electron scattering and, at the lowest (second) order in $\alpha_\pm$, is written (see Appendix A) as

$$\Gamma_\pm(q) = \frac{1}{16}\,\alpha_\pm^2(q)\left(\frac{q}{k_0}\right)^4 \frac{vq\,\sinh\frac{vq}{T}}{\cosh\frac{vq-\mu}{2T}\cosh\frac{vq+\mu}{2T}} . \tag{27}$$

Dynamical screening in the HLL is unusual in two key aspects. First, the very appearance of the plasmon poles in the screened *backscattering* interaction [Eq. (23)] is a rather special feature of the HLL, which distinguishes it—quite apart from the topological protection against elastic backscattering—from the conventional TLL model. The primary property of the HLL that is behind this distinction is that the plasmon excitations (chiral polarization bubbles in the fermionic diagrammatic language) are only coupled to the backscattering interaction, i.e., participate in its screening, by g_5 scattering (see Fig. 7) which, in turn, relies on the existence of a Dirac point. That is, while the $g_{5\perp}$ processes do not, as shown in Sec. III B, contribute to Coulomb drag directly, they influence it by triggering the additional, plasmon-mediated mechanism of electron-electron backscattering.

Second, the plasmon contribution to Coulomb drag is suppressed by the topological nature of the edge states much more weakly than the electron-hole contribution. This can already be inferred from the observation that $1/\tau_D^\infty$ in Eq. (21), being taken with the static interaction potential $V_{12}(q, 0)$, scales with the ultraviolet momentum scale k_0 as $1/k_0^8$, whereas $\Gamma_\pm$ from Eq. (27) scales as $1/k_0^4$. A consequence of this is that the plasmon-mediated Coulomb drag, which is entirely due to dynamical screening, plays a much more prominent role in the HLL compared to more conventional higher-dimensional conductors (for more detail, see Sec. III E).

When integrating over Q, the drag rate in Eq. (21) is represented as a sum of two terms, one coming from the the sum over the "thermal poles" at $Q = \pm q/2 + \mu/v + i\pi(2n-1)T/v$, where n is an integer, the other coming from the "plasmon poles" of $|V_{12}(q, 2vQ)|^2$. In the limit of $\Gamma_\pm(q) \ll T$, with $\Gamma_\pm(q)$ taken at the characteristic q that give the main contribution to $1/\tau_D^\infty$, the two terms can be cleanly separated as, respectively, the electron-hole ($1/\tau_{\rm eh}$) and plasmon ($1/\tau_{\rm p}$) contributions to the drag rate:

$$\frac{1}{\tau_D^\infty} \to \frac{1}{\tau_{\rm eh}} + \frac{1}{\tau_{\rm p}} . \tag{28}$$

These two will be calculated in Secs. III D and III E.

D. Electron-hole contribution to the drag rate

We first calculate $1/\tau_{\rm eh}$, the electron-hole contribution to the drag rate, defined above Eq. (28) and obtainable by neglecting the dynamical part of the screened potential in Eq. (21). To find $1/\tau_{\rm eh}$ for $|\alpha| \ll 1$, we substitute the bare potential $V_{12}(q)$ for the static potential $V_{12}(q, 0)$. The result depends on the relation between three energy scales, T, $|\mu|$, and v/d, all being assumed to be much smaller than the ultraviolet scale of our model vk_0.

In the limit of low T, for $T \ll \min\{v/d, |\mu|\}$, we obtain

$$\text{(I)}: \quad \frac{1}{\tau_{\rm eh}} \simeq \frac{64}{5}\pi\alpha^2\left(\frac{\mu}{vk_0}\right)^8\left(\frac{\pi T}{\mu}\right)^4 T\, e^{-4k_F d} , \quad T \ll \min\{v/d, |\mu|\} . \tag{29}$$

The main contribution to $1/\tau_{\rm eh}$ in this limit comes from $g_{1\perp}$ processes, with the characteristic $|q \pm 2k_F| \sim |Q| \sim T/v$. The drag rate (29) vanishes for $T \to 0$ as T^5. Here

and below, (I), (II), etc. label different transport regimes to be shown in Fig. 3, etc.

In the opposite limit of high T, for $\max\{v/d, |\mu|\} \ll T$, we get

$$\text{(II)}: \quad \frac{1}{\tau_{\rm eh}} \simeq \frac{\pi}{5}(3\pi^4 - 35\pi^2 + 60) \times \pi\alpha^2 \left(\frac{\pi T}{v k_0}\right)^8 \left(\frac{\mu}{\pi T}\right)^2 \left(\frac{v}{\pi T d}\right)^7 T \,, \quad \max\{v/d, |\mu|\} \ll T \,. \quad (30)$$

The contributions of $g_{1\perp}$ and $g_{3\perp}$ processes to Eq. (30)—which are, as already mentioned in Sec. III B, of different sign—strongly compensate each other, with the characteristic $|q| \sim 1/d$ and $|Q| \sim T/v$. The structure of Eq. (30) in the form of a product of four T dependent factors transparently reflects the physics of Coulomb drag in the high-T limit. The T dependence of $1/\tau_{\rm eh}$ that results from this product is seen to cancel out; that is, in the limit of high T, the electron-hole contribution to the drag rate is independent of T.

For T between two other scales, $|\mu|$ and v/d, the result for $1/\tau_{\rm eh}$ reads, depending on which of the two scales is larger:

$$\text{(III)}: \quad \frac{1}{\tau_{\rm eh}} \simeq \frac{512}{315}\left(\frac{22}{15}\pi^2 + 13\right) \times \pi\alpha^2 \left(\frac{\pi T}{v k_0}\right)^8 \left(\frac{\mu}{\pi T}\right)^2 T \,, \quad |\mu| \ll T \ll v/d \,, \quad (31)$$

and

$$\text{(IV)}: \quad \frac{1}{\tau_{\rm eh}} \simeq 18\pi\alpha^2 \left(\frac{\mu}{v k_0}\right)^8 \left(\frac{v}{T d}\right)^4 \frac{1}{(k_F d)^3}\, T\, e^{-\frac{2|\mu|}{T}} \,, \quad v/d \ll T \ll |\mu| \,. \quad (32)$$

In both cases, similarly to Eq. (30), there is a strong compensation between the contributions of $g_{1\perp}$ and $g_{3\perp}$ processes. In both cases, the main contribution to $1/\tau_{\rm eh}$ comes from $|q| \sim 1/d$: the difference is that the characteristic $|Q|$ is given by T/v in Eq. (31) and by k_F in Eq. (32). Note that $1/\tau_{\rm eh}$ in Eq. (32) behaves, with changing T, according to the Arrhenius law with the activation gap $2|\mu|$.

The crossover between the limits $T \ll v/d \ll |\mu|$ and $v/d \ll T \ll |\mu|$ [Eqs. (29) and (32), respectively] has the form of a sharp singularity at $T = T_c$, where $T_c = v/2d$. Specifically:

$$\text{(V)}: \quad \frac{1}{\tau_{\rm eh}} \simeq 192\pi\alpha^2 \left(\frac{\mu}{v k_0}\right)^8 \left(\frac{T_c}{\mu}\right)^4 T_c \times e^{-\frac{2|\mu|}{T_c}} \left(\frac{T_c}{T_c - T}\right)^6 \,, \quad \frac{v}{k_F d^2} \ll T_c - T \ll T_c \quad (33)$$

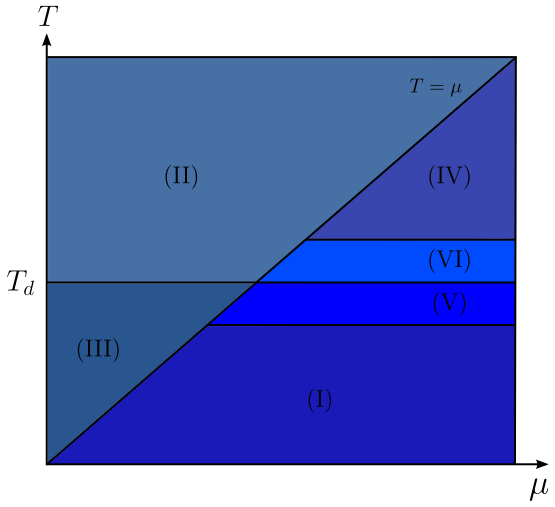

FIG. 3. Electron-hole contribution $1/\tau_{\rm eh}$ to the drag rate, with different regimes in the T–μ plane labeled according to the corresponding equations in Sec. III D. The sequence of different types of the T dependence of $1/\tau_{\rm eh}$, depending on whether the distance d between the edges is larger or smaller than the Fermi wavelength, is shown at the very end of Sec. III D. In the low-T limit, $1/\tau_{\rm eh}$ vanishes at $T \to 0$ as T^5 (regime I). In the high-T limit, $1/\tau_{\rm eh}$ does not depend on T (regime II). In between, $1/\tau_{\rm eh}$ monotonically increases with growing T at fixed μ, with the crossover temperatures given by $|\mu|$ and (as marked on the T axis) $T_d \sim v/d$. For $k_F d \gg 1$, there is a sharp change (regimes V and VI) in the T behavior of $1/\tau_{\rm eh}$ at $T \simeq T_c = v/2d$.

for $T < T_c$ and

$$\text{(VI)}: \quad \frac{1}{\tau_{\rm eh}} \simeq \frac{384}{5}\pi\alpha^2 \left(\frac{\mu}{v k_0}\right)^8 \left(\frac{T_c}{|\mu|}\right)^3 T_c \times e^{-\frac{2|\mu|}{T}} \left(\frac{T_c}{T - T_c}\right)^5 \,, \quad \frac{v}{k_F d^2} \ll T - T_c \ll T_c \quad (34)$$

for $T > T_c$, both in the "critical region" $|T - T_c| \ll T_c$. The broadening of the power-law "resonance" at $T = T_c$ is of the order of $v/k_F d^2 \ll T_c$.

The peculiar behavior of $1/\tau_{\rm eh}$ in Eqs. (33) and (34) is related to the interplay between two exponential factors in the integrand of Eq. (21): $\exp(-2|q|d)$ [from the static interaction potential $V_{12}(q)$] and $\exp(-v|q \pm 2k_F|/2T)$ (from the thermal occupation factors for $T \ll |\mu|$) in the interval $-2k_F < q < 2k_F$. On the low-T [Eq. (33)] and high-T [Eq. (34)] sides of the resonance, the integrand is sharply peaked at $|q| = 2k_F$ and $q = 0$, respectively. Specifically, for Eq. (33), the characteristic momenta are $|q \pm 2k_F| \sim |Q| \sim T_c^2/v(T_c - T)$. For Eq. (34), they are $|q| \sim T_c^2/v(T - T_c)$ and $|Q| \sim k_F$. At the resonance, the q dependence in the exponential factors cancels out and $1/\tau_{\rm eh}$ is determined by $|q| \sim |Q| \sim k_F$. It is worth noting that, despite Eqs. (33) and (34) having the spike-like power-law factors, $1/\tau_{\rm eh}$ is a monotonic function of

T, namely it increases with growing T on both sides of the "spike." This is because the nonsingular (at $T = T_c$) factor $\exp(-2|\mu|/T)$ in Eq. (34) is a faster function of T than the singular factor $[T_c/(T - T_c)]^5$ in the tail of the resonance for $T - T_c \gg v/k_F d^2$.

As T increases, the sequence of different types of the T dependence of $1/\tau_{\rm eh}$—depending on whether $k_F d \gg 1$ or $k_F d \ll 1$—is as follows (see also Fig. 3). For $k_F d \gg 1$, $1/\tau_{\rm eh}$ behaves as

$$T^5 \text{ (I)} \to \text{sharp crossover (V)+(VI)} \to \exp(-2|\mu|/T)/T^3 \text{ (IV)} \to \text{const}(T) \text{ (II)} .$$

For $k_F d \ll 1$, $1/\tau_{\rm eh}$ behaves as

$$T^5 \text{ (I)} \to T^7 \text{ (III)} \to \text{const}(T) \text{ (II)} .$$

In both cases, $1/\tau_{\rm eh}$ is a monotonic function of T, vanishing at $T \to 0$ and saturating in the limit of large T.

E. Plasmon-mediated Coulomb drag

We now turn to the calculation of $1/\tau_{\rm p}$, the plasmon contribution to the drag rate $1/\tau_D^\infty$, as defined above Eq. (28). Taking the residue of the four plasmon poles in the lower half-plane of Q at $Q = (v_\pm/2v)q - i\Gamma_\pm/2v$ and $Q = -(v_\pm/2v)q - i\Gamma_\pm/2v$, we represent $1/\tau_{\rm p}$ for $|\alpha| \ll 1$ as

$$\frac{1}{\tau_{\rm p}} \simeq \frac{\pi^3}{128}\,\alpha^2 \frac{v^5}{T k_0^8} \int_q q^{12} e^{-2|q|d}\, W(q, q/2) \times \sum_\pm \left(1 - \frac{v_\pm^2}{v^2}\right)^4 \frac{1}{\Gamma_\pm} \,\mathrm{Re}\, \frac{1}{\left[(v_+ - v_-)q - i\Gamma_\pm\right]^2 + \Gamma_\mp^2} . \tag{35}$$

In the derivation of Eq. (35), we assumed that the plasmon modes are weakly decaying. More precisely, we used not only the condition $v_\pm|q| \gg \Gamma_\pm$ which is altogether necessary to meaningfully define the plasmon modes in the first place, but a stronger condition $|\alpha_\pm v_\pm q| \gg \Gamma_\pm$. The latter makes it justifiable to neglect the plasmon damping in the factor $q^2 - 4Q^2$ in the numerator of $V_{12}(q, 2Q/v)$ [Eq. (23)] at the plasmon poles in Eq. (21), not requiring at the same time that $|(v_+ - v_-)q|$ is large compared to $\Gamma_\pm$.

The important point here is that the energy splitting between the symmetric and antisymmetric plasmon modes $|(v_+ - v_-)q|$ falls off sharply with increasing $|q|d$, namely as $\exp(-2|q|d)$, so that the broadening of the modes $\Gamma_\pm$—even though being small in the parameter $(q/k_0)^4 \ll 1$ and the additional power of α [Eq. (27)]—can become larger than the splitting for $|q|$ larger than a certain characteristic momentum $q_p \gg 1/d$ (with q_p being still much smaller than k_0). As will be shown below, this circumstance essentially modifies the general picture of plasmon-mediated Coulomb drag, with friction being strongly suppressed by the overlap between the symmetric and antisymmetric plasmon modes. For $(\alpha_+ - \alpha_-)^2 v^2 q^2 \gg |\Gamma_+^2 - \Gamma_-^2|$ (which includes $|q| \sim q_p$), the second line in Eq. (35) can be further simplified to

$$\sum_\pm \frac{4\alpha_\pm^4}{\Gamma_\pm} \frac{1}{(\alpha_+ - \alpha_-)^2 q^2 + 16\Gamma_\pm^2} . \tag{36}$$

Let us first calculate $1/\tau_{\rm p}$ for the case in which the main contribution to $1/\tau_{\rm p}$ comes from $|q| \ll q_p$, i.e., the plasmon damping can be neglected in the "Lorentzian" (36) (recall that $\Gamma_\pm$ is a strong function of q, hence the quotation marks). Importantly, the exponential factor $e^{-2|q|d}$ in Eq. (35) is then canceled by the same factor in $(\alpha_+ - \alpha_-)^2$ from the denominator in Eq. (36), so that the screened interaction effectively extends beyond the scale of $1/d$ in q space. Specifically, Eq. (35) reduces to

$$\frac{1}{\tau_{\rm p}} \simeq \frac{\pi^3}{32}\,\alpha^2 \frac{v^2}{T k_0^4} \frac{\sinh\frac{\mu}{T}}{\cosh^3\frac{\mu}{2T}} \int_q q^5 \left(1 + e^{-2|q|d}\right) \times \frac{1}{\cosh\frac{vq}{2T}} \left[\frac{1}{\cosh\frac{vq-\mu}{2T}} - (q \to -q)\right] . \tag{37}$$

The radius of the bare interaction only remains in the factor $1 + \exp(-2|q|d)$ that originates from the sum $\alpha_+^4 + \alpha_-^4$ and changes between 2 and 1 with increasing $|q|$. Crucially, the strength of interaction cancels out in Eq. (36), so that $1/\tau_{\rm p}$ in Eq. (37) scales with α as α^2, similar to $1/\tau_{\rm eh}$.

In the limit of low T, for $T \ll |\mu| \ll v/d$, we obtain

$$\text{(VII)}: \quad \frac{1}{\tau_{\rm p}} \simeq \frac{\pi^3}{6}\pi\alpha^2 \left(\frac{\mu}{v k_0}\right)^4 \left(\frac{\mu}{\pi T}\right)^2 T\, e^{-|\mu|/T} , \quad T \ll |\mu| \ll v/d . \tag{38}$$

In stark contrast to the electron-hole contribution to the drag rate, which vanishes for $T \to 0$ as a power-law of T, the plasmon contribution in Eq. (38) obeys Arrhenius' law. The main contribution to Eq. (38) comes from all q in the interval $0 < |q| < k_F$.

For $|\mu| \ll T \ll v/d$, we have

$$\text{(VIII)}: \quad \frac{1}{\tau_{\rm p}} \simeq \frac{7\pi^3}{24}\pi\alpha^2 \left(\frac{\pi T}{v k_0}\right)^4 \left(\frac{\mu}{\pi T}\right)^2 T , \quad |\mu| \ll T \ll v/d , \tag{39}$$

with characteristic $|q| \sim T/v$. For $v/d \ll \max\{T, |\mu|\}$, the exponential term $e^{-2|q|d}$ in Eq. (37) can be neglected, so that $1/\tau_{\rm p}$ is obtained by multiplying Eq. (38) (for $T \ll v/d \ll |\mu|$) or Eq. (39) (for $|\mu| \ll v/d \ll T$) by a factor of 1/2.

Now, turn to the case of $\max\{T, |\mu|\} \gg T_p = v q_p/2$, where the plasmon damping substantially modifies plasmon-mediated Coulomb drag. In this limit, $1/\tau_{\rm p}$

can be represented as

$$\frac{1}{\tau_{\rm p}} \simeq \frac{\pi^3}{32}\,\alpha^2\,\frac{v^2}{Tk_0^4}\,\frac{\sinh\frac{\mu}{T}}{\cosh^3\frac{\mu}{2T}}\int_q q^5\frac{1}{s(q)} \times\frac{1}{\cosh\frac{vq}{2T}}\left[\frac{1}{\cosh\frac{vq-\mu}{2T}}-(q\to -q)\right]\,, \quad (40)$$

where

$$s(q)=1+4\alpha^2\left(\frac{2q}{k_0}\right)^8 e^{2|q|d} \times\frac{\sinh^2\frac{vq}{T}}{\cosh^2\frac{vq-\mu}{2T}\,\cosh^2\frac{vq+\mu}{2T}}\,. \quad (41)$$

In fact, Eq. (40) has a broader range of applicability, namely $\max\{T,|\mu|\}\gg v/d$. In particular, it gives, for $s(q)\to 1$, the result that follows from Eq. (37) for $v/d\ll\max\{T,|\mu|\}\ll T_p$, as discussed below Eq. (39). What changes for $\max\{T,|\mu|\}\gg T_p$ is that the function $s(q)$ can no longer be approximated by unity for $|q|\sim\max\{T/v,k_F\}$. Specifically, $1/s(q)$ behaves as a step function: $1/s(q)\to\theta(q_p-|q|)$, falling off sharply with increasing $|q|$, as $e^{-2|q|d}$, for $|q|-q_p\gg 1/d$, where $q_p\gg 1/d$ is defined by $s(q_p)-1\sim 1$. That is, $1/\tau_{\rm p}$ in the limit of strong plasmon damping is determined by all q in the interval $0<|q|<q_p$, with $q_p\ll\max\{T/v,k_F\}$.

We obtain, for three different regimes of plasmon-mediated Coulomb drag in which the plasmon damping is important:

$$\text{(IX)}:\quad \frac{1}{\tau_{\rm p}}\simeq\frac{2}{7\pi}\pi\alpha^2\left(\frac{\pi T}{vk_0}\right)^4\left(\frac{\mu}{\pi T}\right)^2\left(\frac{T_p}{T}\right)^7 T\,, \quad \max\{|\mu|,T_p\}\ll T\,, \quad (42)$$

where

$$T_p=\frac{v}{2d}\ln\left[\frac{(k_0d)^4}{|\alpha|}\,\frac{Td}{v}\right]\,; \quad (43)$$

$$\text{(X)}:\quad \frac{1}{\tau_{\rm p}}\simeq\frac{16}{3\pi^3}\pi\alpha^2\left(\frac{\pi T}{vk_0}\right)^4\left(\frac{T_p}{T}\right)^6 T\,e^{-|\mu|/T}\,, \quad T\ll T_p\ll|\mu|\,, \quad (44)$$

where

$$T_p=\frac{v}{2d}\left\{\frac{|\mu|}{T}+\ln\left[\frac{(k_0d)^4}{|\alpha|}\right]\right\}\,; \quad (45)$$

and

$$\text{(XI)}:\quad \frac{1}{\tau_{\rm p}}\simeq\frac{32}{7\pi^3}\pi\alpha^2\left(\frac{\pi T}{vk_0}\right)^4\left(\frac{T_p}{T}\right)^7 T\,e^{-|\mu|/T}\,, \quad T_p\ll T\ll|\mu|\,, \quad (46)$$

where

$$T_p=\frac{v}{2d}\left\{\frac{|\mu|}{T}+\ln\left[\frac{(k_0d)^4}{|\alpha|}\,\frac{Td}{v}\right]\right\}\,. \quad (47)$$

The term $|\mu|/T$ in Eqs. (45) and (47) for T_p appears because, for $T\ll|\mu|$, the plasmon damping rate obeys the Arrhenius law with the activation gap $|\mu|$. Specifically:

$$\Gamma_\pm(q)\simeq\frac{1}{4}\,\alpha_\pm^2(q)\,T\left(\frac{vq}{T}\right)^2\left(\frac{q}{k_0}\right)^4 e^{-|\mu|/T} \quad (48)$$

for $v|q|\ll T$, which is the condition relevant to Eq. (46), and

$$\Gamma_\pm(q)\simeq\frac{1}{8}\,\alpha_\pm^2(q)\,v|q|\left(\frac{q}{k_0}\right)^4\exp\left(\frac{v|q|-|\mu|}{T}\right) \quad (49)$$

for $T\ll v|q|<|\mu|$ (more precisely, as far as the right condition is concerned, for $|\mu|-v|q|\gg T$), which is the condition relevant to Eq. (44).

The plasmon damping is seen to strongly suppress plasmon-mediated Coulomb drag when the energy splitting between the symmetric and antisymmetric plasmon modes (for $|q|\sim\max\{T/v,k_F\}$) becomes much smaller than their damping rate. Specifically, $1/\tau_{\rm p}$ for $|\mu|\ll T$ is suppressed in Eq. (42) compared to Eq. (39) by the additional factor $(T_p/T)^7\ll 1$. For $T\ll|\mu|$, the suppression factor, compared to Eq. (38), is $(T_p/|\mu|)^6\ll 1$ in Eq. (44) and $(T_p/|\mu|)^6T_p/T\ll 1$ in Eq. (46). In all the cases, $1/\tau_{\rm p}$ vanishes as a power law of T_p with increasing damping rate.

Recall that the energy T_p, being defined in terms of the momentum scale q_p above which the plasmon damping becomes relevant, is a function of T. This means that the crossover temperatures that separate regimes VIII and IX on the one hand and X and XI on the other follow as the solution of the equation $T_p(T)=T$. One of the characteristic scales of T that emerges from this is

$$T_{p0}=\frac{v}{2d}\ln\frac{(k_0d)^4}{|\alpha|}\,. \quad (50)$$

The other is

$$T_{p1}=\frac{T_{p0}}{2}\left(1+\sqrt{1+\frac{v}{2d}\,\frac{|\mu|}{T_{p0}^2}}\right)\,. \quad (51)$$

Depending on the relation between $|\mu|$ and T_{p0}, there are two distinct sequences, with varying T, of different types of the T dependence of $1/\tau_{\rm p}$ (see also Fig. 4). For $|\mu|\ll T_{p0}$, as T is increased, $1/\tau_{\rm p}$ first increases according to the Arrhenius law (VII) and then keeps growing, as T^3 (VIII), before the growth changes to the $1/T^4$ (IX) falloff:

$$e^{-|\mu|/T}/T\ \text{(VII)}\ \to\ T^3\ \text{(VIII)}\ \to\ T^{-4}\ \text{(IX)}\,.$$

For $T_{p0}\ll|\mu|$, the interval of T within which there was the T^3 behavior of $1/\tau_{\rm p}$ in the opposite limit shrinks to

zero. The activation growth of $1/\tau_{\rm p}$ with increasing T [(X) and (XI), with different preexponential factors in the Arrhenius law] is directly followed by the downturn to the $1/T^4$ (IX) behavior:

$$e^{-|\mu|/T}T_p^6(T)/T\ \text{(X)} \to e^{-|\mu|/T}T_p^7(T)/T^2\ \text{(XI)} \to T^{-4}\ \text{(IX)}\ .$$

As can be seen from Fig. 4, the energy T_{p0} also gives the crossover scale for $|\mu|$ when it varies between regimes VIII and X. The temperature T_{p1} as a function of μ [Eq. (51)] gives the boundary between regimes X and XI.

By comparing the results for $1/\tau_{\rm eh}$ (I-VI) on the one hand and $1/\tau_{\rm p}$ (VII-XI) on the other, the most notable differences between the electron-hole and plasmon contributions to the drag rate are the following. First of all, as already noted in Sec. III C, the two are different in the way they scale with the ultraviolet momentum cutoff of our theory, namely $1/\tau_{\rm eh} \propto 1/k_0^8$ and $1/\tau_{\rm p} \propto 1/k_0^4$. This renders $1/\tau_{\rm eh}$ to be much smaller than $1/\tau_{\rm p}$ when the three characteristic energy scales T, $|\mu|$, and v/d are of the same order. Moreover, one can see that $1/\tau_{\rm eh} \ll 1/\tau_{\rm p}$ at $T \sim |\mu|$ for arbitrary $k_F d$. This brings us to the question of differences in the T dependence of $1/\tau_{\rm eh}$ and $1/\tau_{\rm p}$.

One of the differences is that $1/\tau_{\rm p}$ is a nonmonotonic function of T, i.e., in the high-T limit, $1/\tau_{\rm eh}$ is independent of T (II), whereas $1/\tau_{\rm p}$ decreases with increasing T (IX). However, on the side of high T, the plasmon-mediated mechanism of Coulomb drag can be seen to remain dominant, with $1/\tau_{\rm p} \gg 1/\tau_{\rm eh}$ in the whole range of T up to $T \sim vk_0$. The situation is different in the low-T limit. Here, the T dependence of $1/\tau_{\rm p}$ is characterized by the activation gap $|\mu|$ [(VII) and (X)], whereas $1/\tau_{\rm p}$ vanishes at $T \to 0$ as a power law of T. In fact, $1/\tau_{\rm eh}$ also behaves, similarly to $1/\tau_{\rm p}$, according to Arrhenius' law for $T \ll |\mu|$—even with the doubled activation gap $2|\mu|$—if $k_F d \gg 1$, but only within the intermediate interval of T (IV). That is, the "electron-hole mechanism" of Coulomb drag inevitably wins over the plasmon mechanism in the limit of low T, leading to the universal T^5 behavior (I) of the drag rate at $T \to 0$ for arbitrary $k_F d$. One of the conclusions that follow from this comparison is that there necessarily exists a crossover temperature T_1 which separates the electron-hole (lower T) and plasmon-dominated (higher T) regimes of Coulomb drag. Specifically,

$$T_1 = \frac{1}{4}\,\frac{|\mu|}{\ln(k_0/|\mu|) + k_F d}\ . \tag{52}$$

Note that the saturation of the dependence of T_1 with increasing $|\mu|$ occurs at $|\mu| \simeq (v/d)\ln(k_0 d)$, i.e., below T_{p0} [Eq. (50)]. A similar crossover of the drag resistivity between the particle-hole dominated and plasmon-dominated regimes was predicted in the context of two-dimensional heterostructure bilayers of strongly correlated electron liquids, within the Boltzmann-Langevin stochastic kinetic equation approach, in Ref. [44].

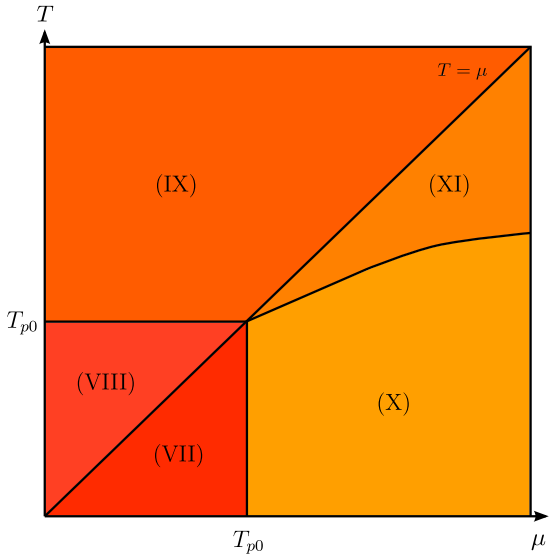

FIG. 4. Plasmon contribution $1/\tau_{\rm p}$ to the drag rate, with different regimes in the T–μ plane labeled according to the corresponding equations in Sec. III E. The sequence of different types of the T dependence of $1/\tau_{\rm p}$, depending on the relation between $|\mu|$ and the characteristic temperature T_{p0} [Eq. (50)], is shown at the end of Sec. III E. In contrast to the electron-hole contribution to the drag rate (Fig. 3), $1/\tau_{\rm p}$ is a nonmonotonic function of T for given μ. In the low-T limit, $1/\tau_{\rm p}$ vanishes at $T \to 0$ according to Arrhenius' law with the activation energy $|\mu|$ (regimes VII and X). In the high-T limit, $1/\tau_{\rm p}$ vanishes with increasing T as T^{-4} (regime IX).

F. DC Coulomb drag

In Secs. III D and III E, we calculated the drag rate in the high-frequency limit $1/\tau_D^\infty$. Now we turn to Coulomb drag in the dc limit, characterized by the dc drag rate $1/\tau_D$ (related to the dc drag resistivity ρ_D by $\rho_D = \pi/e^2 v\tau_D$). Generically, the relaxation rate need not be a constant of ω (when this is the case, at the model level, the system is said to obey the Drude law). In fact, the drag rate is known to be sensitive to the rate of thermal equilibration inside each of the two conductors—to the extent that, while being finite in the high-ω limit, the drag rate may exactly vanish at $\omega \to 0$ if some of the thermalization processes are quenched [34, 45] (see also Refs. [35, 46, 47] for other examples of a failure of the perturbative approach to Coulomb drag). By the same token, the Drude law *is* valid for Coulomb drag if the thermalization rate inside each of the conductors is much larger than the drag rate [34].

In the HLL, the intraedge electron-electron scattering rate $1/\tau_{ee}$, resulting from $g_{5\|}$ interactions, reads [15]

$$\frac{1}{\tau_{ee}} \sim \alpha^2 \left(\frac{T}{v_F k_0}\right)^4 T\,, \qquad |\mu| \lesssim T \tag{53}$$

for $|\mu| \lesssim T$ and

$$\frac{1}{\tau_{ee}} \sim \alpha^2 \left(\frac{\mu}{v k_0}\right)^4 |\mu|\, e^{-|\mu|/T}\,, \qquad T \lesssim |\mu| \tag{54}$$

for $T \lesssim |\mu|$. This is the thermalization rate that should be compared with $1/\tau_D^\infty$ obtained in Secs. III D and III E. For $|\mu| \ll T$, the drag rate is mainly given by $1/\tau_{\rm p}$, which is smaller than $1/\tau_{ee}$ from Eq. (53) by a small factor $(\mu/T)^2$ for $T \ll T_p$ [Eq. (39)] and is further suppressed by plasmon damping [Eq. (42)]. It follows that the dc drag rate $1/\tau_D$ for $|\mu| \ll T$ coincides with $1/\tau_{\rm p}$ calculated in Sec. III E.

For $T \ll |\mu|$, both $1/\tau_{\rm p}$ and $1/\tau_{ee}$ obey Arrhenius' law with the same activation gap $|\mu|$; however, the pre-exponential factors behave with varying T differently. If $|\mu| \ll T_p$, then $1/\tau_{\rm p} \gg 1/\tau_{ee}$ for all $T \ll |\mu|$. Otherwise, the range of T within which $1/\tau_{\rm p} \ll 1/\tau_{ee}$ extends, as follows from Eq. (44), down below $|\mu|$ to $T \gg |\mu|(T_p/\mu)^6$, but $1/\tau_{\rm p}$ still becomes larger than $1/\tau_{ee}$ for lower T. Moreover, in contrast to both $1/\tau_{ee}$ and $1/\tau_{\rm p}$, the drag rate $1/\tau_{\rm eh}$ behaves in the low-T limit as a power law of T [Eq. (29)]. As a result, although $1/\tau_{\rm eh} \ll 1/\tau_{ee}$ at $T \sim |\mu|$ (independently of the parameter $k_F d$), there exists a crossover temperature—much smaller than $|\mu|$—below which the relation between the two scattering rates is reversed. In fact, with logarithmic accuracy, this crossover temperature is given by Eq. (52). Thus, irrespective of the relation between $1/\tau_{ee}$ and $1/\tau_{\rm p}$ at $T \sim |\mu|$, the drag rate is larger than the intraedge thermalization rate in the low T limit. It follows that $1/\tau_D^\infty$ and $1/\tau_D$ need not coincide in this limit.

In fact, in one dimension, the relation between $1/\tau_D^\infty$ and $1/\tau_D$ is largely dictated by the relative strength of backscattering compared to scattering with small momentum transfer. If the latter is dominant, then $1/\tau_D^\infty$ and $1/\tau_D$ can be vastly different from each other, as shown in Ref. [34] for the case of one-dimensional electrons with a parabolic dispersion relation. Otherwise, $1/\tau_D^\infty$ and $1/\tau_D$ are generically of the same order of magnitude, being only different by a numerical coefficient. Below, we demonstrate this by solving the kinetic equation for the HLL in the low-T limit, namely $T \ll v/d \ll |\mu|$. Recall that Umklapp ($g_{3\perp}$) scattering is strongly suppressed for $T \ll |\mu|$ (Sec. III D), so that the only scattering channel that remains (and will only be present in the collision integral below) is $g_{1\perp}$ backscattering. It is also worth noting that forward ($g_{4\perp}$) scattering between chiral electrons is exactly absent in the collision integral for the HLL model with a linear electron spectrum. This is because of the RPA resummation that splits the electron and plasmon velocities in the energy-momentum conservation law and regularizes to zero the collision integral, similarly to the spinful TLL model [48].

The collision integral (10) for $g_{1\perp}$ backscattering ($\eta_1 = -\eta_{1'} = -\eta_2 = \eta_{2'}$) reads

$$\begin{aligned}\mathrm{st}_1(1) = \frac{1}{8vk_0^8}\int_{k_{1'}} V_{12}^2(k_1-k_{1'})(k_1^2-k_{1'}^2)^4\zeta^2(-\eta_1,k_{1'})\\ \times\,[g_1(-\eta_1,k_{1'})+g_2(\eta_1,k_1)\\ -g_1(\eta_1,k_1)-g_2(-\eta_1,k_{1'})]\end{aligned} \tag{55}$$

and $\mathrm{st}_2(1) = -\mathrm{st}_1(1)$, at the lowest order in the static interaction (for $|\alpha| \ll 1$ and $T \ll T_1$). The contribution of intraedge ($g_{5\|}$) scattering to $\mathrm{st}_1(1)$ is neglected in the low-T limit (for $T \ll T_1$). By introducing the functions

$$g_\pm(\eta,k) = \frac{1}{2}\left[\, g_1(\eta,k) \pm g_2(\eta,k)\,\right]\,, \tag{56}$$

we define the total and relative charge components of the distribution function

$$g_\pm^c(k) = \frac{1}{2}\left[\, g_\pm(+,k) - g_\pm(-,-k)\,\right]\,. \tag{57}$$

The drag resistivity can be written as [34]

$$\rho_D = \frac{E_1 - E_2}{j_-}\,, \tag{58}$$

where the relative current $j_- = (j_1 - j_2)/2$ is expressed solely in terms of $g_-^c(k)$:

$$j_- = \frac{ev}{2}\int_k \frac{g_-^c(k)}{\cosh^2\frac{vk-\mu}{2T}}\,. \tag{59}$$

The kinetic equation for g_-^c reads

$$\begin{aligned}-i\omega g_-^c(k_1) - \frac{e(E_1-E_2)v}{2T} &= \mathrm{st}_c(1)\,,\\ \mathrm{st}_c \simeq -\frac{1}{4vk_0^8}\int_{k_{1'}} V_{12}^2(k_1-k_{1'})\,&\frac{(k_1^2-k_{1'}^2)^4}{\cosh^2\frac{vk_{1'}+\mu}{2T}}\\ &\times\left[g_-^c(-k_{1'})+g_-^c(k_1)\right]\,.\end{aligned} \tag{60}$$

For $T \ll |\mu|$, we can replace $k_1 - k_{1'}$ with $2k_F$ in the factors $(k_1^2 - k_{1'}^2)^4$ in the collision integral. Furthermore, for $T \ll v/d$ the argument of the interaction potential can also be set equal to $2k_F$. Note that both these conditions on temperature are satisfied for $T \ll T_1$. Taking the limit $\omega \to 0$, we cast Eq. (60) in the form of a dimensionless integral equation

$$\mathcal{A}(x)\mathcal{G}(x) = 1 - \int \mathrm{d}y\,\frac{(x-y)^4}{\cosh^2 y}\mathcal{G}(y)\,, \tag{61}$$

$$\mathcal{A}(x) = \int \mathrm{d}y\,\frac{(x-y)^4}{\cosh^2 y} = \frac{7\pi^4}{120} + \pi^2x^2 + 2x^4\,, \tag{62}$$

for the function

$$\begin{aligned}\mathcal{G}(x) = \frac{2^7}{\pi}\left(\frac{k_F}{k_0}\right)^4 \frac{V_{12}^2(2k_F)}{v^2}\,&\frac{T^2}{ev(E_1-E_2)}\\ &\times\left(\frac{T}{vk_0}\right)^4 g_-^c\!\left(\frac{2T}{v}x + k_F\right)\,.\end{aligned} \tag{63}$$

The dc drag resistivity is then obtained as

$$\rho_D = \frac{2}{e^2\lambda}\frac{V_{12}^2(2k_F)}{v^2}\left(\frac{2k_F}{k_0}\right)^4\left(\frac{2T}{vk_0}\right)^4 T\,, \tag{64}$$

with the constant

$$\lambda = \int \mathrm{d}x\,\frac{\mathcal{G}(x)}{\cosh^2 x} \simeq 0.242\,. \tag{65}$$

We thus conclude that, for $T \lesssim T_1$, the drag rate that determines the dc drag resistivity is parametrically the same as $1/\tau_D^{\infty}$.

IV. INTRAEDGE INTERACTION: BOSONIZATION FRAMEWORK

In Sec. III, we discussed Coulomb drag between helical edges within the kinetic equation framework and neglected the TLL renormalization effects. Below, we complement the formalism of Sec. III by employing the bosonization approach. In particular, this allows us to proceed to lower temperatures for which the renormalization leads, as is usual in one dimension, to anomalous power-law T dependences of the observables.

Since the renormalization effects in Luttinger liquids necessarily involve backscattering processes, the characteristic temperature scale at which the renormalization starts cannot exceed v/d. Indeed, the distance d between the edges gives the characteristic radius of the interedge interaction potential V_{12}, so that on smaller spatial scales one cannot treat this interaction as local. In fact, in addition to d, screening by external gates introduces another spatial scale d_0 for both the intraedge and interedge interaction, so that the renormalization is only operative for $T \lesssim v/\max\{d, d_0\}$. Below, for simplicity, we assume that $d \sim d_0$.

In what follows, we first bosonize the model and analyze the resulting phase diagram for two coupled helical edges. Next, we discuss the implications of the renormalization effects for the drag resistivity.

A. First-order backscattering

For concreteness, we concentrate on the case of $k_F d \gg 1$. Then, for $T \ll v/d$ (which is, as mentioned above, the range of T where the renormalization is effective) we have also $T \ll |\mu|$, so that the transitions resulting from Umklapp interactions of two particles in the vicinity of the Dirac point are thermally suppressed. Neglecting them, the part of Eq. (4) that describes chirality-changing interactions reduces to backscattering in the vicinity of the Fermi surface. The Hamiltonian density simplifies, then, to $\mathcal{H} = \mathcal{H}_0 + \mathcal{H}_f + \mathcal{H}_b$, where $\mathcal{H}_0$ corresponds to the free Hamiltonian in Eq. (2) and $\mathcal{H}_{f,b}$ describes forward (f) and backward (b) scattering. Moreover, one can describe this type of backscattering by momentum-independent coupling constants determined by the Fourier transform of the interedge and intraedge interaction potentials at the transferred momentum equal to $2k_F$.

To write $\mathcal{H}$, it is convenient to introduce the electron operators at a given point in real space, for the right- and left-moving electrons, in the form

$$\psi_{\sigma+}(x) = R_\sigma(x)e^{ik_F x}, \quad \psi_{\sigma-}(x) = L_\sigma(x)e^{-ik_F x}, \tag{66}$$

where $R_\sigma(x)$ and $L_\sigma(x)$ vary slowly on the scale of k_F^{-1}. Specifically, $\mathcal{H}_0$ and $\mathcal{H}_f$ are written similar to the conventional Luttinger model as

$$\mathcal{H}_0 = -iv\left(R_\sigma^\dagger \partial_x R_\sigma - L_\sigma^\dagger \partial_x L_\sigma\right) \tag{67}$$

and

$$\begin{aligned}\mathcal{H}_f = &\sum_{\sigma\sigma'}\left(g_{2\parallel}\delta_{\sigma\sigma'} + g_{2\perp}\delta_{\sigma,-\sigma'}\right)\rho_{R\sigma}\rho_{L\sigma'} \\ &+ \frac{1}{2}\sum_{\sigma\sigma'\eta}\left(g_{4\parallel}\delta_{\sigma\sigma'} + g_{4\perp}\delta_{\sigma,-\sigma'}\right)\rho_{\eta\sigma}\rho_{\eta\sigma'}\,,\end{aligned} \tag{68}$$

where the chiral densities in $\mathcal{H}_f$ are given by $\rho_{R\sigma} = R_\sigma^\dagger R_\sigma$ and $\rho_{L\sigma} = L_\sigma^\dagger L_\sigma$, and the coupling constants read $g_{4\parallel} = g_{2\parallel} = V_{11}(0)$ and $g_{4\perp} = g_{2\perp} = V_{12}(0)$. The backscattering part

$$\mathcal{H}_b = \sum_{\sigma\sigma'}\left(g_{1\parallel}\delta_{\sigma\sigma'} + g_{1\perp}\delta_{\sigma,-\sigma'}\right)h_\sigma^\dagger h_{\sigma'} \tag{69}$$

is represented in terms of R_σ and L_σ differently, compared to the conventional Luttinger model, with h_σ coming from the spatial gradient expansion:

$$h_\sigma = \left[\,(\partial_x R_\sigma^\dagger)L_\sigma - R_\sigma^\dagger(\partial_x L_\sigma)\,\right]a\,, \tag{70}$$

where a is the ultraviolet cutoff in real space. As discussed above, the local representation of the backscattering term is valid on spatial scales larger than d, hence $a \sim d$. The coupling constants for backscattering are given by

$$g_{1\parallel} = \frac{4k_F^2}{k_0^4 a^2}V_{11}(2k_F), \quad g_{1\perp} = \frac{4k_F^2}{k_0^4 a^2}V_{12}(2k_F). \tag{71}$$

Note that the ultraviolet scale a cancels out in Eq. (69).

The forward scattering term $\mathcal{H}_f$ can be treated exactly by bosonization, with the fermionic fields represented in terms of the bosonic field $\varphi_\sigma(x)$ and its canonical conjugate $\theta_\sigma(x)$ as

$$R_\sigma(x) = \frac{1}{\sqrt{2\pi a}}\,e^{i\sqrt{\pi}[\varphi_\sigma(x) - \theta_\sigma(x)]}\,, \tag{72}$$

$$L_\sigma(x) = \frac{1}{\sqrt{2\pi a}}\,e^{-i\sqrt{\pi}[\varphi_\sigma(x) + \theta_\sigma(x)]}\,. \tag{73}$$

Changing from the "wire basis" ($\sigma = 1, 2$) to the basis of symmetric (+) and antisymmetric (−) fields

$$\varphi_\pm = (\varphi_1 \pm \varphi_2)/\sqrt{2}, \quad \theta_\pm = (\theta_1 \pm \theta_2)/\sqrt{2}, \tag{74}$$

the bosonized Hamiltonian density reads

$$\mathcal{H} = \sum_{\lambda=\pm} \frac{v_\lambda}{2} \left[K_\lambda (\partial_x \theta_\lambda)^2 + K_\lambda^{-1} (\partial_x \varphi_\lambda)^2 \right] + \frac{g_{1\perp}}{\pi} \left[(\partial_x \theta_+)^2 - (\partial_x \theta_-)^2 \right] \cos\left(2\sqrt{2\pi} \varphi_- \right) , \tag{75}$$

where

$$K_\pm = \sqrt{\frac{1-U_\pm}{1+U_\pm}} , \tag{76}$$

$$v_\pm = u_\pm \sqrt{1-U_\pm^2} \tag{77}$$

with

$$U_\pm = \frac{1}{2\pi u_\pm} \left(g_{2\parallel} \pm g_{2\perp} \right) , \tag{78}$$

$$u_\pm = v + \frac{1}{2\pi} \left(g_{4\parallel} \pm g_{4\perp} \right) . \tag{79}$$

Note that for $g_{2\parallel} \pm g_{2\perp} = g_{4\parallel} \pm g_{4\perp}$, the relation $v_\pm K_\pm = v$ holds.

In the bosonized Hamiltonian (75), we have disregarded the terms arising due to the intraedge backscattering ($g_{1\parallel}$-terms), since they contain the fourth power of gradients and hence are highly irrelevant in the infrared. This should be contrasted with the conventional Luttinger liquid, where such terms can be fully incorporated by shifting $g_{2\parallel}$.

Because of the $g_{1\perp}$ scattering processes, the coupling constants for the double-edge system described by the Hamiltonian (75) are subject to renormalization. Under a renormalization-group (RG) transformation that keeps the quadratic term in Eq. (75) invariant, the scaling dimension for the backscattering operator is obtained as $2(K_- - 1) + 2$, with $2(K_- - 1)$ describing the renormalization of the cosine term and the second term coming from the spatial gradients. That is, backscattering is irrelevant in the RG sense, with the coupling constant

$$\alpha_b = \frac{g_{1\perp}}{2\pi v_-} \tag{80}$$

scaling with T as

$$\alpha_b(T) = \alpha_{b0} \left(\frac{Td}{v} \right)^{2K_-} , \tag{81}$$

where α_{b0} in the bare coupling.

It is worth noting that the renormalization of $g_{1\perp}$ here is governed by the forward-scattering amplitudes encoded in K_-, in contrast to the conventional spinful Luttinger liquid, where the backscattering is renormalized by itself (more precisely, the weak-coupling beta function for $g_{1\perp}$ is proportional to the product $g_{1\perp} g_{1\parallel}$) [49]. The difference stems from the inequality $g_{2\perp} \neq g_{2\parallel}$ that gives $K_- < 1$ for spatially distant edges and from the strong irrelevance of the $g_{1\parallel}$ interaction.

We will return to the scaling behavior of "first-order backscattering" in Sec. IV C, when calculating ρ_D. For now, we proceed with the RG treatment of Eq. (75). The discussion above brought up an important point that the theory with $\mathcal{H}$ from Eq. (75) is weakly coupled, *provided* no additional couplings that become relevant are generated by the RG transformation. In fact, as we discuss in Sec. IV B, second-order backscattering processes do become relevant for sufficiently strong forward-scattering interactions.

B. Higher-order backscattering

As already mentioned in Sec. IV A, the backscattering operator in Eq. (75), which is itself irrelevant, can generate relevant operators under the RG transformation. These describe higher-order backscattering processes. Among the additional backscattering terms in the rescaled Hamiltonian, the relevancy is the highest for the term proportional to the next-order, compared to Eq. (75), harmonic of the field φ_-, i.e., to $\cos(4\sqrt{2\pi}\varphi_-)$. Importantly, the emergent additional backscattering interaction is not suppressed by spatial gradient terms in the prefactor of the cosine, in contrast to Eq. (75). Specifically, as shown in Appendix B, the perturbative (in $\alpha_b \ll 1$) RG yields the $\cos(4\sqrt{2\pi}\varphi_-)$ term at the second order in $g_{1\perp}$. The resulting effective action reads $S = S_0 + S_1 + S_2$, where

$$\begin{aligned} S_0 =& \sum_{\lambda=\pm} \int \mathrm{d}x \mathrm{d}\tau \, \{ -i \partial_x \theta_\lambda \partial_\tau \varphi_\lambda \\ &+ \frac{v_\lambda}{2} \left[K_\lambda (\partial_x \theta_\lambda)^2 + \frac{1}{K_\lambda} (\partial_x \varphi_\lambda)^2 \right] \Big\} , \\ S_1 =& 2 v_- \alpha_b \int \mathrm{d}x \mathrm{d}\tau \left[(\partial_x \theta_+)^2 - (\partial_x \theta_-)^2 \right] \cos\left(2\sqrt{2\pi} \varphi_- \right) , \\ S_2 =& v_- \beta_b \int \frac{\mathrm{d}x \mathrm{d}\tau}{\pi a^2} \cos\left(4\sqrt{2\pi} \varphi_- \right) . \end{aligned} \tag{82}$$

Here we discarded the highly irrelevant terms stemming from $g_{1\parallel}$ that modify S_0 by introducing terms with higher gradients (in this regard, their effect is similar to the effect of a finite curvature of the electronic dispersion relation). Note that the term S_1 couples the antisymmetric ($-$) sector with the symmetric ($+$) one, but, as discussed above, this term is irrelevant in the RG sense (at least, in the weak-coupling regime). The structure of the term S_2 suggests its interpretation as describing the processes of correlated four-fermion backscattering. A similar term with doubled harmonics is generated under the RG in disordered helical edges, see, e.g., Ref. [15], where it described a two-particle backscattering off the random potential.

Neglecting S_1, the action (82) becomes identical to that for two coupled spinless TLLs, characterized by the Luttinger constant K_-^{TLL} for the antisymmetric field

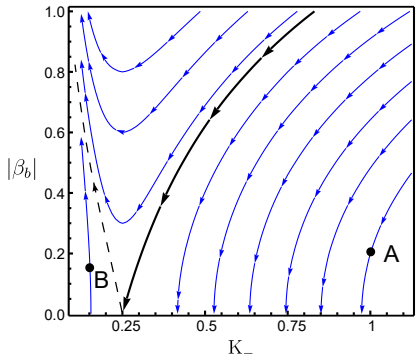

FIG. 5. Renormalization-group flow of the coupling constant for interwire second-order backscattering β_b vs the Luttinger constant for the relative charge mode K_-. The separatrix between the strong- (point B at $K_- < 1/4$) and weak-coupling (point A at $K_- \simeq 1$) phases (thick black line) terminates at a strongly-interacting point with $K_- = 1/4$. To the left of the dashed curve the magnitude of β_b grows monotonously.

$\varphi_-^{\rm TLL}$, if one changes $K_- \to K_-^{\rm TLL}/4$ and rescales $\varphi_- \to \varphi_-^{\rm TLL}/4$. One importance consequence of this mapping is that the system of two strongly correlated helical liquids with $K_- \simeq 1/4$ behaves similarly to weakly interacting TLLs. In particular, there is a Berezinskii-Kosterlitz-Thouless (BKT) transition in the limit of $g \to 0$ at $K_- = 1/4$ [49]. Specifically, the RG equations for the coupling constants K_- and $\beta_b = g/2\pi v_-$, which characterize the action (82), read

$$\frac{dK_-}{d\ell} = -8\beta_b^2 K_-^2 \ , \qquad \frac{d\beta_b}{d\ell} = 2(1-4K_-)\beta_b \ , \qquad (83)$$

where $\ell = \ln(\Lambda_d/\Lambda)$, the ultraviolet cutoff Λ_d in energy space is of the order of v/d, and Λ is the running cutoff.

The bare value of β_b in Eq. (83) is always smaller than the bare value of α_b. Indeed, on the ultraviolet scales $\Lambda \sim \Lambda_d$, the coupling constant β_{b0} is quadratic in $g_{1\perp}$ and proportional to the function $F(K_-, K_+)$ from Eq. (B10). Importantly, the function $F(K_-, K_+)$ is nonzero for $K_\pm > 0$, so that the second-order backscattering is always generated. According to the weak-coupling RG equations (83), the sign of β_b is not changed in the course of the renormalization, while the renormalization of K_- is insensitive to the sign of β_b by Eq. (83). Furthermore, for $|\beta_b| \ll 1$, inelastic processes mediated by second-order backscattering (see Sec. IV C below) are also insensitive to the sign of β_b. Therefore, in what follows, when discussing the weak-coupling regime, we will use the notation β_b for $|\beta_b|$.

The integral curves

$$\beta_b(K_-) = \left[\beta_{b0}^2 + 2\left(\frac{1}{4K_-} - \frac{1}{4K_0} - \ln\frac{K_0}{K_-}\right)\right]^{1/2} \qquad (84)$$

of the RG flow for different initial conditions β_{b0} and K_0 are shown in Fig. 5. The separatrix

$$\beta_b^{(s)}(K_-) = \left[2\left(\frac{1}{4K_-} - 1 - \ln\frac{1}{4K_-}\right)\right]^{1/2} \qquad (85)$$

divides the phase space into the basin of attraction for the line of weak-coupling fixed points with $\beta_b = 0$ and $K_- > 1/4$ (by way of illustration, point A in Fig. 5) and the region in which the flow is to strong coupling (growing β_b with $K_- < 1/4$, point B in Fig. 5)).

Note that the behavior of β_b as a function of T reduces, for $\beta_{b0} \ll 1$, to a simple power law (one can neglect the renormalization of K_-):

$$\beta_b(T) = \beta_{b0}\left(\frac{Td}{v}\right)^{8K_0-2} \ . \qquad (86)$$

For $K_0 < 1/4$, second-order backscattering becomes stronger as T is decreased. The characteristic temperature T^* at which Eq. (83) gives $\beta_b(T^*) \sim 1$ corresponds to the onset of the strong-coupling regime. For the interwire potential specified below Eq. (5), the result for this temperature scale is given by

$$T^* \sim \frac{v}{d}\,\beta_{b0}^{1/(2-8K_-)} \propto \exp\left(-\frac{k_F d}{1-4K_-}\right) \ . \qquad (87)$$

with $K_- = K_0$.

In the strong-coupling limit, the term S_2 in the action (second-order backscattering) tends to lock the phase φ_- at the minima of the cosine potential in Eq. (82), which implies the formation of a charge-density wave in the double-wire system. This is similar to the strong-coupling regime for two conventional spinless Luttinger liquids with repulsive interactions [22, 24]. At the level of the action $S_0 + S_2$, the difference is that there is a threshold value for the strength of repulsive interactions below which the strong-coupling regime cannot be reached in helical liquids, whereas arbitrarily small repulsion between electrons drives the system into the strong-coupling regime in conventional Luttinger liquids. We will discuss Coulomb drag between helical liquids for the case of strong coupling in Sec. IV D.

C. Luttinger-liquid renormalization of the drag resistivity

In this Section, we calculate the drag resistivity by incorporating the power-law renormalization which is characteristic of the Luttinger-liquid physics. The effect of forward scattering ($K_- < 1$) on Coulomb drag mediated by the first-order backscattering (described by the term S_1 in the action) can be taken into account by using a renormalized interaction coupling constant $\alpha_b(T)$ in the results obtained above by means of solving the kinetic equation (Sec. III). This amounts to the replacement

$$V_{12} \to V_{12}\left(\frac{Td}{v}\right)^{2(K_--1)} \qquad (88)$$

in the results of Sec. III F. In particular, for $T \to 0$ this replacement yields

$$\rho_D \sim \frac{1}{e^2}\alpha_b^2(T)\, T \sim \frac{1}{e^2}\alpha_{b0}^2 \left(\frac{Td}{v}\right)^{4K_-} T \propto T^{4K_-+1}. \quad (89)$$

The dependence of the prefactor of the power law on K_- in this expression is obtained in Appendix C.

As pointed out in Sec. IV B, the backscattering operator in Eq. (75), which itself is irrelevant, can generate relevant operators under the RG flow. These describe higher-order backscattering processes that contribute to the drag resistivity at order α_{b0}^4. As we will see below, one cannot neglect these contributions, even though they are of higher order in the bare interedge interaction strength. This is because they may scale with a lower power of T than the first-order backscattering contributions and hence may overcome the lowest-order at sufficiently low T. Moreover, for the case of sufficiently strong interaction (low values of K_-), these contributions lead to the increase of ρ_D with lowering T.

The effect of second-order backscattering is not captured by the kinetic-equation approach developed above, which includes only pair collisions and neglects interedge correlations. To obtain the drag conductivity due to the second-order backscattering processes, we calculate the drag conductivity using the Kubo formula,

$$\sigma_D(\omega) = -\frac{i}{\omega} \lim_{i\Omega_n \to \omega + i0} \lim_{q\to 0} \langle j_1(q,\Omega_n) j_2(-q,-\Omega_n)\rangle \,, \quad (90)$$

where $j_\sigma(x,\tau) = eK_\sigma v_\sigma \partial_x \theta(x,\tau)/\sqrt{\pi}$ is the current in edge $\sigma = 1, 2$. Here, the correlation function is calculated with respect to the action $S = S_0 + S_2$ in Eq. (82), yielding the high-frequency drag conductivity

$$\mathrm{Re}\,\sigma_D(\omega) = \frac{e^2 v_-}{\omega^2}\beta_{b0}^2 \left(\frac{\pi T d}{v_-}\right)^{16K_- -3} \frac{v_-}{d}\Upsilon(K_-)\,,$$
$$\Upsilon(K_-) = \frac{8}{\pi^2}\cos^2(4\pi K_-)\Gamma^2(\tfrac{1}{2} - 4K_-)\Gamma^2(4K_-)\,, \quad (91)$$

where $\Gamma(x)$ is the Euler gamma function.

The total high-frequency drag conductivity is a sum of the contribution due to first-order backscattering and the contribution of Eq. (91). Following the reasoning presented in Sec. III F, we expect that the dc drag resistivity is determined by the high-frequency drag rate extracted from the ac conductivity. A rigorous analysis of the renormalized dc drag resistivity can be performed in a two-step way. First, one renormalizes the bosonized theory down to the energy scale given by T. Second, one refermionizes the theory and solves the kinetic equation for the new fermionic excitations. We relegate this program to future work. Comparing Eq. (91) with Eq. (C9), we see that the second-order contribution scales with a lower power of T when the interedge correlations are sufficiently strong, $K_- < 1/3$. Moreover, as we have already shown, second-order backscattering becomes relevant for $K_- < 1/4$. Then, the weak-coupling analysis performed above is only valid for sufficiently high temperatures.

Summarizing, the low-T drag resistivity is dominated by the first-order backscattering processes, Eq. (C9), as long as $K_- > 1/3$. For stronger repulsive intraedge interaction, $1/4 < K_- < 1/3$, the low-T drag resistivity is governed by second-order backscattering, Eq. (91). At $K_- < 1/4$, these scattering processes become relevant in the RG sense and lead to the increasing drag resistivity as T is lowered.

D. Coulomb drag in the strong-coupling limit

In this section, we discuss the drag resistivity at the strong-coupling fixed point of the RG flow derived in Sec. IV B. We remind the reader that there is a mapping of the bosonized theory described by the action $S_0 + S_2$ (neglecting the irrelevant term S_1) in Eq. (82) to the theory of coupled TLLs with the Luttinger constant $K = 4K_-$. Thus, the problem of Coulomb drag in helical edges in the strong-coupling regime is expected to bear similarity to the drag between spinless TLLs discussed in Ref. [22, 24] and to the problem of pinned charge density waves [50, 51]. To keep our analysis self-contained, we will reproduce here the main results of these works, using the notation of Sec. IV B and only keeping the terms S_0 and S_2 in the bosonized action.

For definiteness, we assume that β_b is positive (for negative β_b the consideration is qualitatively similar). In the strong coupling limit, with $\beta_b \gg 1$ and $K_- \ll 1/4$, the action $S_0 + S_2$ is minimized by the uniform mean-field configurations $\sqrt{32\pi}\varphi_-(x) \equiv \phi_m = (2m+1)\pi$. Recall that φ_- describes the displacement of electrons in wire 2 with respect to electrons in wire 1, so that the mean-field solution gives two interlocked charge density waves. At finite T, there exist massive harmonic fluctuations around this mean-field result. However, these excitations do not carry the antisymmetric current.

Electron transport from one end of the active wire to the other only occurs if the mean-field value of the field changes from ϕ_m to $\phi_{m\pm1}$. Depending on temperature, transitions between the degenerate ground states occur due to either quantum tunneling or thermal activation. The excitations that carry the current are either (anti-)solitons that move along the wire or soliton-antisoliton pairs that are formed inside the wire and dissociate by the applied electric field. The energy E_s and width W_s of a classical soliton are [51]

$$E_s = \sqrt{\frac{2\beta_b}{\pi^2 K_-}}\frac{v_-}{a}\,, \qquad W_s = \frac{1}{4\sqrt{K_-\beta_b}}a\,. \quad (92)$$

When W_s is much smaller than the system length, the response in the antisymmetric sector is determined by the thermal excitation of soliton-antisoliton pairs and reads

as [50]

$$\rho_{\rm therm} = \frac{h}{32\pi e^2 \ell_s}\sqrt{\frac{E_s T a^2}{2\beta K_- v_-}}\, e^{E_s/T}\,, \tag{93}$$

where ℓ_s is the soliton mean free path.

In conventional TLLs, repulsive backscattering interactions between two (spinless) wires always become stronger as T is decreased—for arbitrary bare strength of the interactions. That is, there exists a characteristic temperature T^* at which the coupling constant for electron-electron backscattering becomes of the order of unity. Below T^*, a zigzag-ordered charge density wave is formed, as discussed above. As a consequence, one of the primary properties of Coulomb drag between TLLs with repulsive interwire interactions is that ρ_D shows activation behavior, Eq. (93), for $T \ll T^*$:

$$\ln \frac{\rho_D(T)}{\rho_D(\Delta)} \simeq \frac{\Delta}{T} \tag{94}$$

with the activation gap $\Delta \sim T^*$ [22].

Based on the above mapping, one concludes that for $K_- < 1/4$ the drag resistivity has a local minimum at a characteristic temperature T^*, Eq. (87), at which the coupling constant β_b for the second-order backscattering becomes of the order of unity. Below this temperature, $\rho_D(T)$ starts growing exponentially due to thermally activated transitions between neighboring ground states. On the other hand, if $K_- > 1/4$, this local minimum does not occur and the drag resistivity vanishes as a power law as $T \to 0$.

We emphasize that the above conclusion is based on retaining only the terms S_0 and S_2 in the bosonized action (82). If the mapping onto the conventional theory of 1D Coulomb drag worked for the helical edges, for $K_- < 1/4$ one would obtain $\rho_D = -\rho_{12} \to \infty$ at $T \to 0$. However, from the general structure of the resistivity tensor, it follows that the diagonal (intraedge) resistivity should diverge simultaneously: $\rho_{11} \to \infty$. Indeed, for clean (no disorder) systems we have $\rho_{11} = -\rho_{12}$. Thus, the divergence of the drag resistivity would mean that the interedge coupling destroys the topological protection of the (otherwise) conducting helical edge states. Specifically, on both sides of the quantum spin-Hall transition driven by the closing and reopening of the gap in the 2D bulk of the system (gap inversion), we would then have nonconducting edge states. However, at zero gap, the 2D bulk state is still conducting; therefore, the delocalized bulk state should transform into the conducting edge state at one side of the QSH transition.

We speculate that, within the framework of an effective edge theory, this "topological protection" might be related to the difference between the HLL and normal TLL: the former contains the additional term S_1 in the action ("α-term"). While in the weak-coupling regime this term is highly irrelevant, when the "β-term" S_2 enters the strong-coupling limit, the α-term might again become important, destroying the charge density wave. In this scenario, the topological protection is maintained due to the competition of the α and β terms in the action, leading to nonperturbative effects in the strong-coupling regime. A somewhat similar situation was encountered in Ref. [52] devoted to the 2D surface states of a 3D topological insulator. There, the perturbative (weak-coupling) RG suggested a localization of the surface states, due to the Altshuler-Aronov-type corrections, but the nonperturbative effect of the topological protection resulted in the emergence of a critical state in the strong-coupling regime [53].

To conclude this section, the behavior of ρ_D for sufficiently strong intraedge interaction, namely $K_- < 1/4$, is expected to be governed by the interplay of the tendency to the formation of a charge density wave because of second-order backscattering (the term S_2 in the action) on the one hand and the topological protection (encoded in the α-term S_1) on the other. This interplay might lead to a nonmonotonic T dependence of ρ_D at low T, with a local minimum around T^* and a local maximum at yet lower T. The behavior of ρ_D at finite T would then demonstrate an "apparent metal-insulator transition" with decreasing K_-. Based on the weak-coupling RG formalism, we cannot make definite conclusions about the nature of zero-T Coulomb drag for $K_- < 1/4$. We relegate the corresponding analysis to future work.

V. SUMMARY

We have presented a theory of Coulomb drag between clean (no disorder) helical Luttinger liquids based on the kinetic equation approach supplemented with bosonization to take into account Luttinger liquid renormalization. We have assumed that the spin-rotational invariance of the helical liquid is broken by Rashba spin-orbit coupling in the bulk of the topological insulator, which allows for interedge backscattering events without breaking time-reversal symmetry. We have obtained a richer phase diagram for Coulomb drag in helical liquids compared to conventional 1D wires with repulsive interactions.

A peculiar feature of Coulomb drag between helical liquids—related to the existence of the Dirac point—is exposed in the high-T case. We have shown that Coulomb drag between helical liquids is mediated not only by backscattering but also by Umklapp processes. In the helical liquid, Umklapp scattering is special in that the energy and momentum conservation makes it necessary for one of the involved states (either initial or final) of Umklapp-scattered particles to be right at the Dirac point (see Fig. 2). The Umklapp processes reveal themselves in Coulomb drag between helical liquids in a subtle manner. Their direct contribution to the drag resistivity ρ_D, actually, vanishes exactly; nonetheless, they impact Coulomb drag profoundly by providing for coupling to plasmon modes. In turn, Coulomb drag is dominated by

the excitation of plasmons, triggered by Umklapp scattering. This results in a nonmonotonic T dependence of ρ_D, characterized by several crossovers. In particular, in the limit of high T, the drag resistivity falls off in a universal manner as

$$\rho_D \propto \alpha_{b0}^2\, T^{-4}, \tag{95}$$

where α_{b0} describes the strength of interedge backscattering.

In helical liquids, backscattering is much weakened by spin-momentum locking, and one important question pertinent to the behavior of ρ_D in the low-T limit, where Luttinger-liquid effects become important, is about the outcome of a competition between strong correlations and the spin-momentum locking. The impact of the Luttinger renormalization on the drag resistivity is twofold. First, it renormalizes the power-law exponents in the temperature dependence of ρ_D, depending on the strength of interactions characterized by the Luttinger parameter K_- of the relative charge mode. Second, for $K_- < 1/4$, higher-order electron-electron backscattering processes become strong below a characteristic temperature scale T^* and tend to form a charge density wave. We have shown that, if repulsive interactions are not too strong, namely $K_- > 1/4$, the spin-locking wins and ρ_D vanishes at $T \to 0$ as a power law of T:

$$\rho_D \propto \begin{cases} \alpha_{b0}^2 \left(\frac{T}{T_d}\right)^{4K_- +1}, & K_- > 1/3\ , \\ \alpha_{b0}^4 \left(\frac{T}{T_d}\right)^{16K_- -3}, & 1/3 > K_- > 1/4\ . \end{cases} \tag{96}$$

For $K_- < 1/4$, the system enters the strong-coupling regime at $T \lesssim T^*$. We expect a nonmonotonic behavior of ρ_D as T is lowered further, governed by the interplay between the formation of the charge density wave on the one hand and the topological protection on the other, with a local minimum in the T dependence of ρ_D at $T \sim T^*$ and a local maximum at yet lower T.

Summarizing, the overall picture of the dependence of ρ_D on T, as follows from the results of Secs. III D–IV D, is illustrated in Fig. 6. Viewed from a general perspective, Fig. 6 demonstrates that Coulomb drag between helical liquids is, as already emphasized above, peculiar in two important aspects. One of the peculiarities, apparent in Fig. 6, is that ρ_D vanishes with decreasing T as a power law if intraedge interactions are not too strong. The other, highly unusual, property of helical liquids that we explored in this paper is the peculiar Umklapp-triggered plasmon-mediated mechanism of Coulomb drag that governs the behavior of ρ_D for higher temperatures. This behavior clearly distinguishes Coulomb drag in helical liquids from drag in conventional 1D quantum liquids and could be used to identify helical liquids in Coulomb-drag experiments [54].

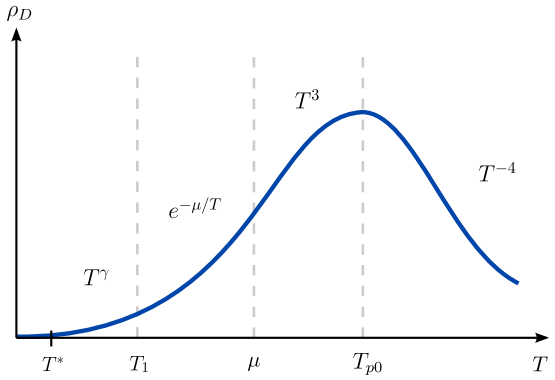

FIG. 6. Sketch of the T dependence of the drag resistivity ρ_D for two helical liquids for $v/d \ll |\mu| \ll T_{p0}$, where T_{p0} [Eq. (50)] is the temperature above which the plasmon damping leads to a strong suppression of the drag rate. For $T \gg T_1$ [Eq. (52)], electron-hole excitations in two edges couple to each other through plasmon modes ("plasmon-mediated Coulomb drag"). For $T \ll T_1$, Coulomb drag is determined by direct backscattering of electrons close to the Fermi surface. The exponent γ in the power-law T dependence of ρ_D at $T \to 0$ is given by $\gamma = 4K_- + 1$ for $K_- > 1/3$ and $\gamma = 16K_- - 3$ for $1/4 < K_- < 1/3$. For $K_- < 1/4$, as T decreases, the system enters the strong-coupling regime at $T \sim T^*$ (Sec. IV B).

VI. ACKNOWLEDGEMENTS

This work was supported by the DFG SPP 1666 "Topological insulators" and by the EU Network FP7-PEOPLE-2013-IRSES under Grant No. 612624 "InterNoM." NK thanks the Carl-Zeiss-Stiftung for financial support. The work at University of Wisconsin-Madison was financially supported in part by NSF Grants No. DMR-1606517, No. ECCS-1560732, and by the Wisconsin Alumni Research Foundation. We acknowledge discussions with C. Brüne, H. Buhmann, S.T. Carr, Y.-Z. Chou, M. Foster, A.D. Mirlin, and B. Trauzettel.

Appendix A: Polarization operator and RPA interaction for the helical edge states

In this Appendix, we derive the polarization operator and the dynamically screened RPA interaction for a homogeneous HLL. The density of helical fermions in edge σ is written as

$$\rho_\sigma(q) = \sum_{\eta_1\eta_2} \int_k \psi^\dagger_{k+q,\eta_1\sigma} \psi_{k\eta_2\sigma} b_{\eta_1\eta_2}(k+q,k)\,, \tag{A1}$$

with the matrix elements $b_{\eta_1\eta_2}(k_1,k_2)$ defined in Eq. (5). The (bare) polarization operator in the Matsubara representation,

$$\Pi(q, i\Omega_m) = -\left\langle \rho(q, i\Omega_m)\rho(-q, -i\Omega_m)\right\rangle \tag{A2}$$

(given that we have identical edges and no tunneling between them, the index σ is dropped here and below),

averaged over the noninteracting ground state, is a sum $\Pi = \sum_{\eta_1\eta_2} \Pi_{\eta_1\eta_2}$ of the chiral components

$$\Pi_{\eta\eta}(q, i\Omega_m) = -T\sum_n \int_k G_{0\eta}(k+q, i\omega_n + i\Omega_m) G_{0\eta}(k, i\omega_n) \quad \text{(A3)}$$

and the backscattering components

$$\Pi_{\eta,-\eta}(q, i\Omega_m) = -T\sum_n \int_k G_{0,-\eta}(k+q, i\omega_n + i\Omega_m) \times G_{0\eta}(k, i\omega_n) b_{\eta,-\eta}(k, k+q) b_{-\eta,\eta}(k+q, k)\,, \quad \text{(A4)}$$

where the bare fermion propagator reads

$$G_{0\eta}(k) = (-i\omega_n + v\eta k - \mu)^{-1}\,. \quad \text{(A5)}$$

We have, then,

$$\Pi_{\eta\eta}(q, i\Omega_m) = \frac{1}{2\pi v}\frac{v\eta q}{v\eta q - i\Omega_m} \quad \text{(A6)}$$

and

$$\Pi_{\eta,-\eta}(q, i\Omega_m) = -\frac{1}{k_0^4}\int_k \frac{\left[k^2 - (k+q)^2\right]^2}{i\Omega_m + 2v\eta k + v\eta q} \times \left[\, n_F(v\eta k) - n_F(-v\eta k - v\eta q)\,\right]. \quad \text{(A7)}$$

After the analytical continuation to real frequencies $i\Omega_m \to \Omega + i0$, the retarded backscattering polarization operator $\Pi_{\eta,-\eta}(q,\Omega)$ is given by

$$\mathrm{Re}\,\Pi_{\eta,-\eta}(q,\Omega) = -\frac{1}{2\pi v}\frac{q^2}{v^2k_0^4}\,\mathcal{P}\int_{-vk_0}^{vk_0} d\epsilon\,\frac{(2\epsilon+\epsilon_q)^2}{2\epsilon+\epsilon_q+\Omega}\,n_F(\epsilon+\mu) + (\Omega\to-\Omega)\,, \quad \text{(A8)}$$

$$\mathrm{Im}\,\Pi_{\eta,-\eta}(q,\Omega) = \frac{1}{4v}\frac{(vq)^2\Omega^2}{(vk_0)^4}\frac{\sinh\frac{\Omega}{2T}}{\cosh\frac{\Omega}{2T} + \cosh\frac{v\eta q+2\mu}{2T}}\,, \quad \text{(A9)}$$

where $\mathcal{P}$ denotes the principal value, $\epsilon = v\eta k$, and $\epsilon_q = v\eta q + 2\mu$. Note that the real part of the backscattering polarization operator diverges at the ultraviolet momentum scale k_0 as k_0^2 (with the dynamical part diverging logarithmically in k_0) while having k_0^{-4} in front of the integral, which means that the contribution of $\Pi_{\eta,-\eta}$ to $\mathrm{Re}\,\Pi$ is much smaller than that of $\Pi_{\eta\eta}$, so that $\mathrm{Re}\,\Pi$ can be approximated (we do not directly use the Kramers-Kronig relation for Π anywhere in the paper) as

$$\mathrm{Re}\,\Pi(q,\Omega) \simeq \frac{1}{\pi v}\frac{(vq)^2}{(vq)^2 - \Omega^2}\,. \quad \text{(A10)}$$

For the imaginary part of Π, we have

$$\mathrm{Im}\,\Pi(q,\Omega) = \frac{\Omega}{2v}\left[\,\delta(vq-\Omega) + \delta(vq+\Omega)\,\right] + \frac{1}{4v}\frac{(vq)^2\Omega^2}{(vk_0)^4}\sinh\frac{\Omega}{2T}\left[\frac{1}{\cosh\frac{\Omega}{2T} + \cosh\frac{vq+2\mu}{2T}} + (q\to-q)\right]. \quad \text{(A11)}$$

We now turn to the calculation of the dynamically screened RPA interaction. The intra- and interedge components of the interaction, $V_{11}(q,\Omega)$ and $V_{12}(q,\Omega)$, respectively, obey the Dyson equation

$$\begin{pmatrix} V_{11} & V_{12} \\ V_{12} & V_{11}\end{pmatrix} = \begin{pmatrix} U_\parallel & U_\perp \\ U_\perp & U_\parallel\end{pmatrix} - \begin{pmatrix} U_\parallel & U_\perp \\ U_\perp & U_\parallel\end{pmatrix}\begin{pmatrix} \Pi & 0 \\ 0 & \Pi\end{pmatrix}\begin{pmatrix} V_{11} & V_{12} \\ V_{12} & V_{11}\end{pmatrix}, \quad \text{(A12)}$$

where $U_\parallel(q)$ and $U_\perp(q)$ are the bare interactions. Solution to Eq. (A12) reads

$$V_{11} = \frac{U_\parallel + \Pi\,(U_\parallel^2 - U_\perp^2)}{1 + 2\Pi U_\parallel + \Pi^2(U_\parallel^2 - U_\perp^2)}\,, \quad \text{(A13)}$$

$$V_{12} = \frac{U_\perp}{1 + 2\Pi U_\parallel + \Pi^2(U_\parallel^2 - U_\perp^2)}\,. \quad \text{(A14)}$$

Within the model, as discussed below Eq. (5), we assume that $U_\parallel(q) = V_0$ is independent of q and $U_\perp(q) = V_0 e^{-|q|d}$. The interedge RPA interaction $V_{12}(q,\Omega)$ can then be written as

$$V_{12}(q,\Omega) = \frac{1}{e^{|q|d}\left[\,V_0^{-1} + 2\Pi(q,\Omega)\,\right] + 2V_0\sinh(|q|d)\,\Pi^2(q,\Omega)}\,. \quad \text{(A15)}$$

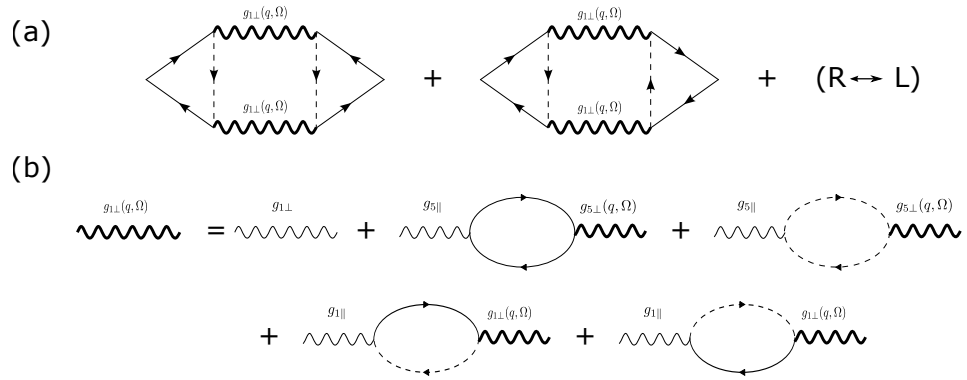

FIG. 7. (a) Aslamazov-Larkin diagrams describing the lowest order contribution to drag. The solid (dotted) lines refer to quasiparticle Greens functions of right (left) movers and the wiggly line denotes the dynamically screened RPA interaction. (b) Diagrammatic representation of the Dyson equation for $g_{1\perp}$ type interaction. We note that the coupling to plasmons (chiral polarization bubbles) is due to g_5 type interaction lines unique to the helical Luttinger liquid. In both (a) and (b) we have set $g_{1,\parallel} = g_{3,\parallel}$ and $g_{1,\perp} = g_{3,\perp}$.

Neglecting $(\mathrm{Im}\,\Pi)^2$ compared to $(\mathrm{Re}\,\Pi)^2$ in the real part of the term Π^2 in the denominator of Eq. (A15) and using $\mathrm{Re}\,\Pi$ from Eq. (A10), $V_{12}(q,\Omega)$ reduces to

$$V_{12}(q,\Omega) = \frac{V_0 e^{-|q|d}[(vq)^2 - \Omega^2]^2}{(\Omega^2 - \Omega_+^2)(\Omega^2 - \Omega_-^2) + 2i(\mathrm{Im}\,\Pi)V_0[(vq)^2 - \Omega^2]^2\left[1 + 2e^{-|q|d}\sinh(|q|d)(\mathrm{Re}\,\Pi)V_0\right]}\,, \tag{A16}$$

where the plasmon modes $\Omega_\pm(q)$ are obtained as the solution of the equation

$$[(vq)^2 - \Omega^2]^2 + 2\alpha(vq)^2[(vq)^2 - \Omega^2] + 2\alpha^2 e^{-|q|d}\sinh(|q|d)(vq)^4 = 0 \tag{A17}$$

with $\alpha = V_0/\pi v$, which gives $\Omega_\pm(q)$ in Eqs. (24)–(26).

Taking the plasmon damping into account, the denominator of Eq. (A16) with the inclusion of the term proportional to $\mathrm{Im}\,\Pi$ is expressible as

$$\left\{[\,\Omega + i\Gamma(q,\Omega)\,]^2 - \Omega_+^2(q)\right\}\left\{[\,\Omega + i\Gamma(q,\Omega)\,]^2 - \Omega_-^2(q)\right\}\,. \tag{A18}$$

In the limit of weak damping, $|\Gamma_+ - \Gamma_-| \ll |\Omega_+(q) - \Omega_-(q)|$, where

$$\Gamma_\pm = \Gamma(q,\Omega_\pm)\,, \tag{A19}$$

this reduces to

$$\left[(\Omega + i\Gamma_+)^2 - \Omega_+^2\right]\left[(\Omega + i\Gamma_-)^2 - \Omega_-^2\right]\,, \tag{A20}$$

as in Eq. (23).

Appendix B: Second-order backscattering

In this Appendix, we perform a real-space RG procedure using the operator product expansion [55] (OPE) to derive the most relevant operator generated by the backscattering term in Eq. (75):

$$S_1 = \frac{g_{1\perp}}{\pi}\int \mathrm{d}x\mathrm{d}\tau\,\cos\left(\sqrt{8\pi}\varphi_-\right)\left[\,(\partial_x\theta_+)^2 - (\partial_x\theta_-)^2\,\right]\,. \tag{B1}$$

The general form for an OPE for two operators $\mathcal{O}_i$ and $\mathcal{O}_j$ is

$$:\mathcal{O}_i(\boldsymbol{r}_{\lambda,1}):\,:\mathcal{O}_j(\boldsymbol{r}_{\lambda,2}):$$
$$= \sum_k \frac{c_{ijk}}{|\boldsymbol{r}_{\lambda,1} - \boldsymbol{r}_{\lambda,2}|^{\Delta_i+\Delta_j-\Delta_k}} : \mathcal{O}_k\left(\frac{\boldsymbol{r}_{\lambda,1} + \boldsymbol{r}_{\lambda,2}}{2}\right) : \tag{B2}$$

where $:\mathcal{O}:$ denotes normal ordering, Δ_i is the scaling dimension of $\mathcal{O}_i$, and $\boldsymbol{r}_\lambda = (x, v_\lambda\tau)^T$ denotes coordinates in space-time. The above equality does not hold on the level of operators, but it is valid when used within the correlation functions, i.e., when the averaging is performed with another set of operators, at a distance much larger than $|\boldsymbol{r}_1 - \boldsymbol{r}_2|$ from $\boldsymbol{r}_1$ or $\boldsymbol{r}_2$.

It is convenient to introduce the complex coordinates $(\bar{z}_\lambda)$ and (z_λ) as

$$z_\lambda = v_\lambda\tau + ix\,, \qquad \bar{z}_\lambda = v_\lambda\tau - ix\,, \tag{B3}$$

where $\tau = -it$ is the imaginary time variable. We further introduce the short-hand notations $1_\lambda \equiv (z_{\lambda,1}, \bar{z}_{\lambda,1})$ and

$z_{\lambda,12} \equiv z_{\lambda,1} - z_{\lambda,2}$. By expanding the partition function of the model defined in Eq. (75) in powers of $g_{1\perp}$, followed by the reexponentiation, we find the effective action [55] to the second order in the coupling constant,

$$S_2 = \frac{1}{2}\left[\langle S_{1\perp}\rangle^2 - \langle S_{1\perp}^2\rangle \right], \tag{B4}$$

where $\langle \ldots \rangle$ denotes the averaging with respect to the fixed-point action. Within the RG procedure, we increase the short-distance cutoff a at each step by an infinitesimal amount, $a \to a' = (1+\ell)a$, which reproduces the action, but with renormalized coupling constants, and may lead to the emergence of new operators. To study the terms in the effective action, we need the time-ordered $\varphi_\lambda\varphi_\lambda$ correlation function of the $\lambda = \pm$ fields,

$$\langle \varphi_\lambda(z_\lambda, \bar{z}_\lambda)\varphi_\lambda(0,0)\rangle = -\frac{K_\lambda}{4\pi}\ln\left[\frac{|z_\lambda|^2 + a^2}{a^2}\right]. \tag{B5}$$

The correlation function for the θ_λ fields can be obtained by using the duality relations

$$K_\lambda \partial_{z_\lambda}\theta_\lambda = \partial_{z_\lambda}\varphi_\lambda\ , \quad K_\lambda \partial_{\bar{z}_\lambda}\theta_\lambda = -\partial_{\bar{z}_\lambda}\varphi_\lambda\ , \tag{B6}$$

which, similarly to the OPE, hold when used for the averages that produce the correlation functions.

The most relevant perturbation in the effective action (B4) is obtained by contracting all $\partial_x\theta$ terms for small space time distances $a < |z_{-,12}| < a'$. Using the correlation function of the bosonic fields and the duality relations (B6), we find the OPEs

$$\begin{aligned}
&\left[(\partial_x\theta_+)^2\, e^{i\sqrt{8\pi}\varphi_-}\right]_1 \left[(\partial_x\theta_+)^2\, e^{i\sqrt{8\pi}\varphi_-}\right]_2 \\
&\to \frac{1}{4(\pi K_+)^2}\frac{(z_{+,12}^2 + \bar{z}_{+,12}^2)^2}{(a^2+|z_{+,12}|^2)^4}\left(\frac{|z_{-,12}|^2+a^2}{a^2}\right)^{2K_-} \\
&\quad \times e^{i\sqrt{8\pi}[\varphi_-(1_-)+\varphi_-(2_-)]},
\end{aligned} \tag{B7}$$

and

$$\begin{aligned}
&\left[(\partial_x\theta_-)^2\, e^{i\sqrt{8\pi}\varphi_-}\right]_1 \left[(\partial_x\theta_-)^2\, e^{i\sqrt{8\pi}\varphi_-}\right]_2 \\
&\to \frac{1}{(4\pi)^2}\Big[\frac{2}{K_-^2}\frac{(z_{-,12}^2+\bar{z}_{-,12}^2)^2}{(a^2+|z_{-,12}|^2)^4} + 4\frac{(z_{-,12}+\bar{z}_{-,12})^4}{(a^2+|z_{-,12}|^2)^4} \\
&\quad - \frac{8}{K_-}\frac{(z_{-,12}+\bar{z}_{-,12})^2}{(a^2+|z_{-,12}|^2)^2}\frac{z_{-,12}^2+\bar{z}_{-,12}^2}{(a^2+|z_{-,12}|^2)^2}\Big] \\
&\quad \times \left(\frac{|z_{-,12}|^2+a^2}{a^2}\right)^{2K_-} e^{i\sqrt{8\pi}[\varphi_-(1_-)+\varphi_-(2_-)]}.
\end{aligned} \tag{B8}$$

Here, we neglected less relevant terms in the OPE. We perform the integration over the relative coordinates by introducing the polar coordinates $z_{-,12} = re^{-i\phi}$ and $z_{+,12} = re^{-i\phi} + r\tilde{v}\cos\phi$ with the parameter $\tilde{v} = v_+/v_- - 1 = K_-/K_+ - 1$. The radial and angular integrations decouple and we perform the radial integration over an infinitesimal shell $r \in (a, a')$ by setting $r = a$. After integrating out the relative coordinates, we obtain the following contribution to the effective action:

$$\delta S_2 = \frac{g_{1,\perp}^2 F(K_-,K_+)\ell}{(2\pi)^2 v_-}\int\frac{\mathrm{d}x\mathrm{d}\tau}{\pi a^2}\,\cos[\sqrt{32\pi}\varphi_-(x,\tau)]\ , \tag{B9}$$

with the dimensionless function

$$F(K_-,K_+) = 2^{2K_-}\left[f_1(K_-,K_+) + f_2(K_-)\right]\ , \tag{B10}$$

where

$$\begin{aligned}
f_1(x,y) =& 4y^2\int_0^{2\pi}\frac{\mathrm{d}\phi}{2\pi}\frac{\left[(x^2+y^2)\cos^2\phi - y^2\right]^2}{\left[2y^2+(x^2-y^2)\cos^2\phi\right]^4} \\
=& \frac{5x^6+45x^4y^2+7x^2y^4+7y^6}{32\sqrt{2}(x^2+y^2)^{7/2}}
\end{aligned} \tag{B11}$$

and

$$\begin{aligned}
f_2(x) =& \frac{1}{(4x)^2}\int_0^{2\pi}\frac{\mathrm{d}\phi}{2\pi}\left[1-4x+6x^2\right. \\
&\left. -8x(1-x)\cos 2\phi + (1-4x+2x^2)\cos 4\phi\right] \\
=& \frac{1-4x+6x^2}{16x^2}\ .
\end{aligned} \tag{B12}$$

Importantly, the function $F(K_-,K_+)$ is nonzero for $K_\pm > 0$. We thus see that, upon renormalization, the new coupling constant is always generated in the effective action, even if it is absent at the ultraviolet scale. The effect of the term (B9) on the phase diagram of capacitively coupled helical edge modes is discussed in Sec. IV B.

Appendix C: Renormalization of the drag resistivity

In this Appendix, we derive the asymptotics of the drag resistivity at $T \to 0$ for $K_- > 1/3$. We assume for simplicity that the interedge interaction is weak. To the lowest order in the interwire interaction, the dc drag resistivity can be expressed as [27, 32]:

$$\rho_D = \int_0^\infty \mathrm{d}q \int_0^\infty \mathrm{d}\omega\, \frac{q^2 V_{12}^2(q)}{4\pi^3 n_1 n_2 T}\frac{\mathrm{Im}\Pi_1(q,\omega)\mathrm{Im}\Pi_2(q,\omega)}{\sinh^2\left(\frac{\omega}{2T}\right)}, \tag{C1}$$

where $\mathrm{Im}\Pi_\sigma(q,\omega)$ is the imaginary part of the retarded density-density correlation function of wire $\sigma = 1,2$ and $n_\sigma = K_\sigma k_F/\pi$ is the electron density of wire σ. The drag resistivity obtained by this conventional formula is equivalent to that obtained from the high-frequency drag conductivity using the kinetic equation approach [34].

We write the density operator of helical fermions by employing the expansion in Eq. (3). This yields

$$\rho_\sigma(x) = \psi^\dagger_{\sigma,\uparrow}\psi_{\sigma,\uparrow} + \psi^\dagger_{\sigma,\downarrow}\psi_{\sigma,\downarrow} \simeq R^\dagger_\sigma R_\sigma + L^\dagger_\sigma L_\sigma + \frac{2k_F}{k_0^2}\Big\{ i\left[(\partial_x R^\dagger_\sigma)L_\sigma - R^\dagger_\sigma \partial_x L_\sigma\right] e^{-i2k_F x} + \text{H.c.}\Big\}. \tag{C2}$$

The polarization operators entering Eq. (C1) are calculated in the presence of the intrawire interaction which would lead to the Luttinger-liquid renormalization of the drag resistivity, but neglecting correlations between the edges. This amounts to setting $g_{2\perp} = 0$ and $g_{4\perp} = 0$. Then the quadratic part of the total Hamiltonian separates into two independent sectors in the edge basis. As in the main text, we will restrict the discussion to equal edges with Luttinger parameter $K_1 = K_2 \equiv K$ (or, equivalently, $K_- = K_+ = K$) and plasmon velocity $v_1 = v_2 \equiv v$. In the bosonic language, the $2k_F$-part of the density-density correlation function, which determines the behavior of the drag resistivity at low temperatures, can be cast in the form

$$\Pi^{2k_F}(x,\tau) = \frac{4k_F^2}{\pi a^2 k_0^4} e^{-i2k_F x} \times \langle \partial_x\theta(x,\tau)\partial_x\theta(0,0) e^{i\sqrt{4\pi}[\varphi(x,\tau)-\varphi(0,0)]}\rangle + \text{H.c.}\,. \tag{C3}$$

The analytic continuation to real time and the Fourier transform to the frequency-momentum space is standard [49] and yields

$$\Pi^{2k_F}(q,\omega) = \tilde{\Pi}^{2k_F}(q+2k_F,\omega) + \tilde{\Pi}^{2k_F}(q-2k_F,\omega) \tag{C4}$$

with $\tilde{\Pi}^{2k_F}(q,\omega)$ given by

$$\tilde{\Pi}^{2k_F}(q,\omega) = -\left(\frac{k_F}{k_0}\right)^2 \frac{1}{(k_0 a)^2}\left(\frac{\pi a T}{v}\right)^{2K} \frac{1}{\pi^4 T^2} \times \mathcal{K}_K\left(\frac{qv}{4\pi T}, \frac{\omega}{4\pi T}\right). \tag{C5}$$

Here

$$\mathcal{K}_K(x,y) = \left(\frac{1}{K}+1\right)\mathcal{I}_{K+2,2}(x,y) - 2\mathcal{I}_{K,0}(x,y) + \mathcal{J}_{K+1}(x,y) \tag{C6}$$

and we have defined the functions

$$\mathcal{I}_{\gamma,\delta}(x,y) = \sin(\pi\gamma)2^{2\gamma-\delta-2} \times B\left(-i(x+y)+\frac{\gamma-\delta}{2}, -\gamma+\delta+1\right) \times B\left(-i(y-x)+\frac{\gamma}{2}, -\gamma+1\right) + (x\to -x), \tag{C7}$$

and

$$\mathcal{J}_\gamma(x,y) = \frac{v}{(\pi T)^2} 2^{2\gamma-4}\sin(\pi\gamma) \times\Big\{\Big[B\left(-i(x+y)+\frac{\gamma}{2}-\frac{1}{2}, -\gamma+1\right) + B\left(-i(x+y)+\frac{\gamma}{2}+\frac{1}{2}, -\gamma+1\right)\Big] \times\Big[B\left(-i(y-x)+\frac{\gamma}{2}-\frac{1}{2}, -\gamma+1\right) + B\left(-i(y-x)+\frac{\gamma}{2}+\frac{1}{2}, -\gamma+1\right)\Big]\Big\}, \tag{C8}$$

where $B(x,y)$ is the Euler beta-function. When deriving this result, we used

$$\int_0^\infty \mathrm{d}X\, e^{-\mu X}\sinh^\nu(\gamma X) = \frac{1}{2^{\nu+1}\gamma} B\left(\mu/2\gamma - \nu/2, \nu+1\right),$$

where the identity holds as long as $\mathrm{Re}\gamma > 0$, $\mathrm{Re}\nu > -1$ and $\mathrm{Re}\mu > \mathrm{Re}(\gamma\nu)$. In our problem, there exist integrals for which the condition $\mathrm{Re}\nu > -1$, which ensures the infrared convergence, is not fulfilled. In that case, the integrals over time t are cut off at small t by a/v and, consequently, the integrals over X are cut off by $\pi T a/v$.

For $T \to 0$, the function $\mathrm{Im}\,\mathcal{K}\left([q-2k_F]/4\pi T, \omega/4\pi T\right)$ is strongly peaked around $q = 2k_F$ with a width of the peak of the order of T/v. Therefore, we can neglect the term $\mathrm{Im}\,\mathcal{K}_K\left([q+2k_F]/4\pi T, \omega/4\pi T\right)$ in the integral over positive momenta in Eq. (C1). Then, we find

$$\rho_D \sim I_K \frac{[V_{12}(2k_F)]^2}{u^2}\left(\frac{k_F}{k_0}\right)^4 \frac{T}{(k_0 a)^4}\left(\frac{\pi a T}{u}\right)^{4K}, \tag{C9}$$

where

$$I_K = \int_0^\infty \mathrm{d}\Omega\, \frac{[\,\mathrm{Im}\,\mathcal{K}_K(0,\Omega/4\pi)\,]^2}{\sinh^2(\Omega/2)}$$

with $\Omega = \omega/T$. As discussed in the main text, the natural ultraviolet cutoff here is provided by the distance between the edges, $a \sim d$. The parametric dependence of the drag resistivity obtained by means of bosonization reproduces in the limit $K \to 1$ the result (64) of the kinetic-equation analysis.

[1] C. L. Kane and E. J. Mele, Phys. Rev. Lett. **95**, 146802 (2005).

[2] C. L. Kane and E. J. Mele, Phys. Rev. Lett. **95**, 226801

(2005).
[3] B. A. Bernevig and S.-C. Zhang, Phys. Rev. Lett. **96**, 106802 (2006).
[4] M. Z. Hasan and C. L. Kane, Rev. Mod. Phys. **82**, 3045 (2010).
[5] X. Qi and S.-C. Zhang, Rev. Mod. Phys. **83**, 1057 (2011).
[6] J. Maciejko, T. L. Hughes, and S.-C. Zhang, Annu. Rev. Condens. Matter Phys. **2**, 31 (2011).
[7] M. König, S. Wiedmann, C. Brüne, A. Roth, H. Buhmann, L. W. Molenkamp, X.-L. Qi, and S.-C. Zhang, Science **318**, 766 (2007).
[8] A. Roth, C. Brüne, H. Buhmann, L. W. Molenkamp, J. Maciejko, X.-L. Qi, and S.-C. Zhang, Science **325**, 294 (2009).
[9] I. Knez, R.-R. Du, and G. Sullivan, Phys. Rev. Lett. **107**, 136603 (2011).
[10] I. Knez, C. T. Rettner, S.-H. Yang, S. S. P. Parkin, L. Du, R.-R. Du, and G. Sullivan, Phys. Rev. Lett. **112**, 026602 (2014).
[11] L. Du, I. Knez, G. Sullivan, and R.-R. Du, Phys. Rev. Lett. **114**, 096802 (2015).
[12] T. L. Schmidt, S. Rachel, F. von Oppen, and L. I. Glazman, Phys. Rev. Lett. **108**, 156402 (2012).
[13] Reference [12], while studying inelastic backscattering in a helical edge with broken spin-axial symmetry, admits the existence of inelastic backscattering also in models that preserve this symmetry. We believe, however, that inelastic backscattering in a helical edge is only possible if the spin-locking axis changes its orientation with varying k. In particular, the earlier works [2, 19] cited in Ref. [12] also tacitly rely on broken spin-axial symmetry in the context of a nonzero backscattering rate.
[14] N. Lezmy, Y. Oreg, and M. Berkooz, Phys. Rev. B **85**, 235304 (2012).
[15] N. Kainaris, I. V. Gornyi, S. T. Carr, and A. D. Mirlin, Phys. Rev. B **90**, 075118 (2014).
[16] Y.-Z. Chou, A. Levchenko, and M. S. Foster, Phys. Rev. Lett. **115**, 186404 (2015).
[17] H.-Y. Xie, H. Li, Y.-Z. Chou, and M. S. Foster, Phys. Rev. Lett. **116**, 086603 (2016).
[18] The emergence of a nonzero conductivity in a helical liquid at finite T, because of Umklapp scattering, was mentioned in Ref. [2].
[19] C. Wu, B. A. Bernevig, and S.-C. Zhang, Phys. Rev. Lett. **96**, 106401 (2006).
[20] T. Li, P. Wang, H. Fu, L. Du, K. A. Schreiber, X. Mu, X. Liu, G. Sullivan, G. A. Csáthy, X. Lin, and R.-R. Du, Phys. Rev. Lett. **115**, 136804 (2015).
[21] K. Flensberg, Phys. Rev. Lett. **81**, 184 (1998).
[22] Y. V. Nazarov and D. V. Averin, Phys. Rev. Lett. **81**, 653 (1998).
[23] V. V. Ponomarenko and D. V. Averin, Phys. Rev. Lett. **85**, 4928 (2000).
[24] R. Klesse and A. Stern, Phys. Rev. B **62**, 16912 (2000).
[25] A. Komnik and R. Egger, Eur. Phys. J. B **19**, 271.
[26] B. Trauzettel, R. Egger, and H. Grabert, Phys. Rev. Lett. **88**, 116401 (2002).
[27] M. Pustilnik, E. G. Mishchenko, L. I. Glazman, and A. V. Andreev, Phys. Rev. Lett. **91**, 126805 (2003).
[28] P. Schlottmann, Phys. Rev. B **69**, 035110 (2004).
[29] T. Fuchs, R. Klesse, and A. Stern, Phys. Rev. B **71**, 045321 (2005).
[30] G. A. Fiete, K. Le Hur, and L. Balents, Phys. Rev. B **73**, 165104 (2006).
[31] J. Peguiron, C. Bruder, and B. Trauzettel, Phys. Rev. Lett. **99**, 086404 (2007).
[32] D. N. Aristov, Phys. Rev. B **76**, 085327 (2007).
[33] A. V. Rozhkov, Phys. Rev. B **77**, 125109 (2008).
[34] A. P. Dmitriev, I. V. Gornyi, and D. G. Polyakov, Phys. Rev. B **86**, 245402 (2012).
[35] A. P. Dmitriev, I. V. Gornyi, and D. G. Polyakov, Phys. Rev. B **94**, 085404 (2016).
[36] P. Debray, P. Vasilopoulos, O. Raichev, R. Perrin, M. Rahman, and W. Mitchel, Physica E **6**, 694 (2000).
[37] P. Debray, V. Zverev, O. Raichev, R. Klesse, P. Vasilopoulos, and R. S. Newrock, J. Phys.: Condens. Matter **13**, 3389 (2001).
[38] P. Debray, V. N. Zverev, V. Gurevich, R. Klesse, and R. S. Newrock, Semicond. Sci. Technol. **17**, R21 (2002).
[39] M. Yamamoto, M. Stopa, Y. Tokura, Y. Hirayama, and S. Tarucha, Physica E **12**, 726 (2002).
[40] M. Yamamoto, M. Stopa, Y. Tokura, Y. Hirayama, and S. Tarucha, Science **313**, 204 (2006).
[41] D. Laroche, G. Gervais, M. P. Lilly, and J. L. Reno, Nat. Nanotechnol. **6**, 793 (2011).
[42] D. Laroche, G. Gervais, M. P. Lilly, and J. L. Reno, Science **343**, 631 (2014).
[43] V. A. Zyuzin and G. A. Fiete, Phys. Rev. B **82**, 113305 (2010).
[44] W. Chen, A. V. Andreev, and A. Levchenko, Phys. Rev. B **91**, 245405 (2015).
[45] B. N. Narozhny and A. Levchenko, Rev. Mod. Phys. **88**, 025003 (2016).
[46] M. Schütt, P. M. Ostrovsky, I. V. Gornyi, and A. D. Mirlin, Phys. Rev. B **83**, 155441 (2011).
[47] B. N. Narozhny, M. Titov, I. V. Gornyi, and P. M. Ostrovsky, Phys. Rev. B **85**, 195421 (2012).
[48] A. G. Yashenkin, I. V. Gornyi, A. D. Mirlin, and D. G. Polyakov, Phys. Rev. B **78**, 205407 (2008).
[49] T. Giamarchi, *Quantum Physics in One Dimension* (Oxford University Press, Oxford, 2004).
[50] M. J. Rice, A. R. Bishop, J. A. Krumhansl, and S. E. Trullinger, Phys. Rev. Lett. **36**, 432 (1976).
[51] K. Maki, Phys. Rev. Lett. **39**, 46 (1977).
[52] P. M. Ostrovsky, I. V. Gornyi, and A. D. Mirlin, Phys. Rev. Lett. **105**, 036803 (2010).
[53] In this paper, we restrict ourselves to the analysis of the RG equations derived at the lowest order in the couplings α_b and β_b. The next-order terms in the beta functions might give rise to a precursor of the topological protection already in the weak-coupling regime (for $K_- \ll 1$).
[54] Experimentally, the study of Coulomb drag between helical liquids can be performed either with the vertical setup consisting of two parallel quantum wells, as shown schematically in Fig. 1, or with the horizontal setup (C. Brüne and H. Buhmann, private communication), where the two quantum wells are located in the same plane.
[55] J. L. Cardy, *Scaling and renormalization in statistical physics* (Cambridge University Press, 2002).